Vol. 731: 27–49, 2024
https://doi.org/10.3354/meps14329

MARINE ECOLOGY PROGRESS SERIES
Mar Ecol Prog Ser

Published March 13[§]

Contribution to the Theme Section 'Marine functional connectivity'

Integration of empirical and modelled data unravels spatiotemporal distribution and connectivity patterns of Fuegian sprat early life stages

Virginia A. García Alonso[1,2,*], Bárbara C. Franco[3,4,5], Elbio D. Palma[6,7], Marcelo Pájaro[8], Fabiana L. Capitanio[1,2]

[1]Universidad de Buenos Aires, Facultad de Ciencias Exactas y Naturales, Departamento de Biodiversidad y Biología Experimental (DBBE), Buenos Aires C1428EGA, Argentina

[2]CONICET-Universidad de Buenos Aires, Instituto de Biodiversidad y Biología Experimental y Aplicada (IBBEA), Buenos Aires C1428EGA, Argentina

[3]Facultad de Ciencias Exactas y Naturales, Universidad de Buenos Aires, Buenos Aires C1428EGA, Argentina

[4]Centro de Investigaciones del Mar y la Atmósfera (CIMA), CONICET–Universidad de Buenos Aires, Buenos Aires C1428EGA, Argentina

[5]Instituto Franco-Argentino para el Estudio del Clima y sus Impactos (UMI 3351 IFAECI)/CNRS-IRD-CONICET-UBA, Buenos Aires C1428EGA, Argentina

[6]Departamento de Física, Universidad Nacional del Sur, Bahía Blanca B8000FTN, Argentina

[7]Instituto Argentino de Oceanografía (IADO), CONICET-UNS, Bahía Blanca B8000FWB, Argentina

[8]Instituto Nacional de Investigación y Desarrollo Pesquero (INIDEP), Mar del Plata B7602HSA, Argentina

ABSTRACT: The distribution patterns of fish early life stages are critical to recruitment success and closely related to major oceanographic circulation patterns. We explored the spatiotemporal distribution of early life stages of Fuegian sprat *Sprattus fuegensis*, a key trophic species in the Southwestern Atlantic Ocean (SWAO), in a complex oceanographic setting. Samples were collected during austral spring, summer, and autumn, from 2014 to 2017, across areas with distinct biophysical properties between Tierra del Fuego (TDF) and the marine protected area 'Namuncurá' at Burdwood Bank (BB) (ca. 54° S). Results revealed significant seasonal fluctuations in abundance, distribution, and ontogenetic composition across habitats. High egg and early larval abundances at Isla de los Estados (IE) suggest it is an additional spawning ground to those previously identified at TDF and BB. However, only the latter appear to be suitable nursery areas. Particle-tracking simulations based on egg abundance and spawning dates were conducted for the first time using results from a high-resolution hydrodynamic model. Particle transport provides evidence of connectivity between IE and neighbouring areas — enhanced when horizontal diffusivity is incorporated into the model — but not between TDF and BB. Simulated distributions closely resembled empirical patterns from this and other studies, allowing the integration of empirical and modelled data to schematize the species' dispersal pathways in the study area. These results offer new insights into distribution and connectivity patterns among spawning grounds and highlight the potential use of hydrodynamic models for future assessments of Fuegian sprat and other planktonic species' dispersal and recruitment in the SWAO.

KEY WORDS: Fuegian sprat · Early life stages · Spatiotemporal distribution · Particle tracking · Dispersal · Connectivity · Southwest Atlantic Ocean

*Corresponding author: garciaalonso.v.a@gmail.com

[§]Advance View was available July 20, 2023; with a subsequent update February 6, 2024

Publisher: Inter-Research · www.int-res.com

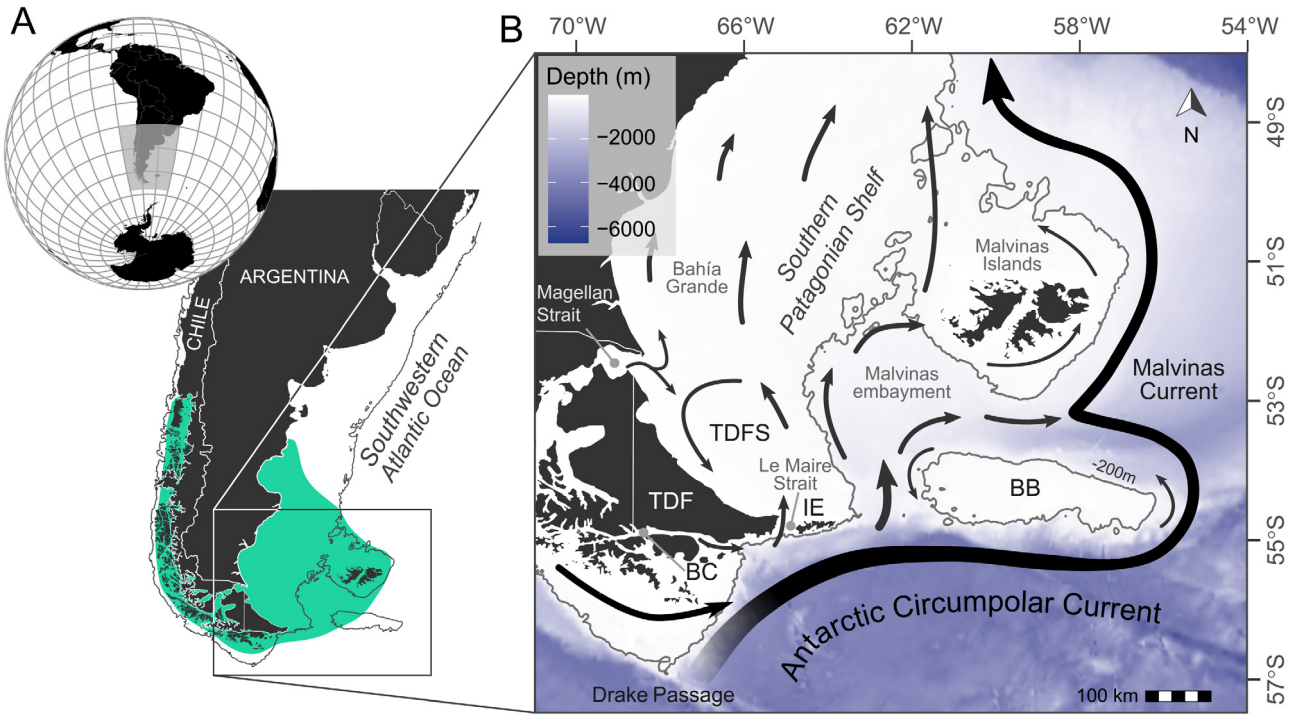

Fig. 1. (A) Fuegian sprat distribution in southern South America (marked in green) following Cousseau (1982) and Cerna et al. (2014), and (B) schematic representation of main oceanographic currents in the Southwestern Atlantic Ocean and Southern Patagonian Shelf following Matano et al. (2019) and Palma et al. (2021). Habitats included in the present study are shown: Tierra del Fuego (TDF), comprising the Beagle Channel (BC) and the continental shelf east of TDF (TDFS), Isla de los Estados (IE), and the marine protected area 'Namuncurá' at Burdwood Bank (BB). Bathymetry retrieved from ETOPO1 Global Relief Model (Amante & Eakins 2009)

1. INTRODUCTION

Small pelagic fishes constitute the largest species group harvested worldwide (FAO 2020) and serve as a critical link within marine food webs of productive ecosystems (Cury et al. 2000). Their dynamics are highly susceptible to ocean–atmosphere variability (Alheit & Hagen 2001, Peck et al. 2013), and changes in their distribution challenge the application of appropriate management strategies, impacting both fish stocks and dependent fisheries (Baudron et al. 2020). Hydrographical features play a crucial role in this regard, defining the early-stage drift pathways and retention areas critical to the match–mismatch dynamics experienced after hatching (Houde 2008, Peck et al. 2012a) and ultimately influencing recruitment success (Baumann et al. 2006a, Romagnoni et al. 2020). Projections suggest that suitable spawning habitats for small pelagic fishes will shift towards higher latitudes (Lima et al. 2022), emphasizing the need to understand the interplay between early-stage dynamics and major circulation patterns to evaluate potential changes in their distribution.

The Fuegian sprat *Sprattus fuegensis* (also called Patagonian, Austral or Falkland sprat) is a small pelagic fish found along the coasts of southern South America (Fig. 1A) (Cousseau 1982, Cerna et al. 2014). This clupeid plays a crucial trophic role at the wasp-waist level in the Southwestern Atlantic Ocean (SWAO) (Riccialdelli et al. 2020) and is vital prey for species of ecological importance (e.g. humpback whales; Acevedo & Urbán 2021) and other commercially exploited species (e.g. long tail hake *Macruronus magellanicus*; Alvarez et al. 2022). Fuegian sprats are furthermore considered one of the main unexploited pelagic resources of the SWAO (Bellisio et al. 1979, Casarsa et al. 2019), thus indirectly conferring them economic importance. Spawning and nursery grounds of this species in the SWAO are known to be located south of 50°S at (1) the Malvinas (Falkland) Islands, (2) the southern region of the Southern Patagonian Shelf (SPS), consisting of the southern and eastern coasts of Tierra del Fuego (TDF), and (3) the Burdwood Bank (BB) (Sánchez et al. 1995, García Alonso et al. 2018). The latter is a submarine plateau located east of TDF, constituting Argentina's first open-sea marine protected area, named 'Namuncurá' (MPA Namuncurá–Burdwood Bank; National Law No. 26875, Argentina).

Fuegian sprats found between TDF and BB — the southernmost location of clupeids worldwide (Sánchez et al. 1997) — are exposed to an extremely complex oceanographic setting (Fig. 1B). The northernmost part of the Antarctic Circumpolar Current (ACC) at Drake Passage plays a key role in the south and east of the mentioned area, transporting cold, relatively fresh (salinity [S] = 34) and nutrient-rich Subantarctic waters through the shelf break. One branch of the ACC turns north at the tip of Isla de los Estados (IE) and then turns east after colliding with the Malvinas Islands Shelf. A second branch of the ACC flows eastwards and follows the southern shelf break of the BB. The 2 branches join north of 52° S to form the Malvinas Current (Piola & Gordon 1989, Palma et al. 2021). In addition to this strong current, a broad anticyclonic current is observed around the edge of BB, forming an active centre for the upwelling of nutrient-rich water into the surface layers (Matano et al. 2019). Along the Beagle Channel (BC) and the continental shelf south of TDF (Cape Horn Shelf), the mean flow is eastward until it reaches the Le Maire Strait or the eastern tip of IE (Balestrini et al. 1998), where it turns north (Guihou et al. 2020). In this region, located onshore from the 200 m isobath, water is strongly affected by continental runoff, glacial melting, and heavy rainfall, with salinities as low as 29.5 in the BC (Brun et al. 2020). As a result, a well-defined salinity front is found between TDF and BB, with the strongest gradient to the east of IE (Acha et al. 2004). Empirical measurements also indicate west–east gradients of temperature and chlorophyll that vary seasonally between the eastern tip of IE and BB (Guerrero et al. 1999). Thus, early life stages of the Fuegian sprat in this region are exposed to varying thermohaline and biological conditions that can influence their distribution, development, and recruitment.

The distribution patterns of Fuegian sprat early stages have been assessed largely based on empirical information gathered from planktonic samples. However, due to logistic and economic constraints, the level of resolution attainable is often limited, thus hampering the ability to characterise spatial and temporal patterns and identify possible changes. Alternative methodological approaches offer potential solutions to these constraints. For instance, particle-tracking simulations based on numerical hydrodynamic models have been successful in predicting dispersal and retention patterns of fish early stages, as well as detecting associations between larval dispersion and recruitment success variability (e.g. Baumann et al. 2006b, Ospina-Alvarez et al. 2015). Combining such models with empirical observations can hence be a powerful tool to assess biological variations within the proposed ecosystem.

Despite the ecological and economic relevance of the Fuegian sprat, a full understanding of the species' distribution patterns and connectivity across habitats during its early life stages is still limited owing to outdated and scattered information. Most studies addressing the early life stages rely on information gathered over 20 yr ago and mainly in TDF (Sánchez & Ciechomski 1995, Sánchez et al. 1995). However, several oceanographic surveys have been conducted in recent years through the Argentine Government's 'Pampa Azul' initiative, providing updated and simultaneous acquisition of oceanographic and planktonic samples between TDF and BB for the first time. These surveys have led to the recognition of a key spawning ground at BB (García Alonso et al. 2018) and the identification of differences in some early life traits among sprat larvae from TDF and BB (García Alonso et al. 2020, 2021). Moreover, the planktonic samples collected from these studies comprise a unique data set for studying distribution and connectivity patterns through both empirical information and particle-tracking simulations. The main objectives of the present study were therefore (1) to simultaneously analyse the spatio-temporal patterns of distribution and abundance of Fuegian sprat early life stages across areas with diverse physical and biological properties between TDF and BB; (2) to conduct passive particle-tracking simulations based on empirical data across the main spawning areas during the spawning peak; and (3) to evaluate the spatial correlation between modelled and empirical data for the species. Through the simultaneous use of empirical and modelled data, we aim to gain new and relevant insights into the distribution and connectivity patterns of Fuegian sprat early life stages and thus better understand the influence of regional circulation patterns on the species' dynamics within these nursery areas. Such insights can serve to support the use of hydrodynamic models in future studies on Fuegian sprat early life stages or any other planktonic organisms in the region.

2. MATERIALS AND METHODS

2.1. Oceanographic surveys

A total of 138 oceanographic stations were sampled across 7 oceanographic cruises, covering 3 cohorts of Fuegian sprat early stages (Table 1). The cruises

Table 1. General information of the oceanographic surveys and nets used to capture Fuegian sprat considered in this study. N: number of sampling stations, X: type of net(s) used

Year	Oceanographic vessel	Dates (dd/mm)	Season	Cohort	N	Net		
						Mini-Bongo	Bongo	IKMT
2014	ARA Puerto Deseado	29/03–14/04	Autumn	–	8		X	
2014	ARA Puerto Deseado	04/11–27/11	Spring	2014–2015	17		X	
2015	SB-15 Tango	17/02–23/02	Summer	2014–2015	11	X		
2015	GC-189 Prefecto García	01/12–17/12	Spring	2015–2016	15	X		
2016	ARA Puerto Deseado	26/03–25/04	Autumn	2015–2016	27		X	
2016	ARA Puerto Deseado	06/12–15/12	Spring	2016–2017	23		X	
2017	ARA Puerto Deseado	22/04–12/05	Autumn	2016–2017	37		X	X

were carried out by the ARA 'Puerto Deseado' oceanographic vessel and the SB-15 'Tango' and GC-189 'Prefecto García' Argentine coastguard vessels during austral spring (2014, 2015, and 2016), summer (2015), and autumn (2014, 2016, and 2017). Most sampling designs included a transect from the BC to the Marine Protected Area 'Namuncurá' at BB, with additional stations at the continental shelf east of TDF (TDFS). Hauls were performed using a 60 cm diameter Bongo net with a 300 µm mesh size, except during the 2015 cruises when a Mini-Bongo net with a 20 cm diameter and a 200 µm mesh size was used. In 2017, an IKMT net was employed to capture juvenile individuals more effectively (Fey 2015). All samples were obtained through oblique tows for 5 min at 2–3 knots from 180 m to the surface or less, reaching bottom proximities between 5 and 10 m when possible. A mechanical flow meter was added to the net mouth in every trawl, and the volume of filtered water was estimated. Samples were fixed in 4% formaldehyde, 80% alcohol, or frozen for further analyses, including both otolith microanalyses and other physiological studies.

Oceanographic stations were assigned to 4 main zones: TDF, IE, BB, and an intermediate zone between IE and BB, west of BB (WBB) (Fig. 2A). This classification was based on bathymetric differences, prevailing oceanographic characteristics (including salinity and temperature gradients; Fig. 2B), and prior knowledge of the species, to be further elaborated on below. Stations classified as TDF are located at the western limit of the area, including both the BC and TDFS, forming part of the Magellanic regime ($S < 33$); previous studies have described a spatial connection between these environments for early stages of a unique Fuegian sprat population (Sánchez et al. 1997). Stations around IE and along the shelf to its north (delimited by the 200 m isobath) constitute another zone under higher salinity influences ($33.4 < S < 33.8$). The remaining area is part of the Subantarctic regime ($33.9 < S < 34.3$; minimum temperature). Owing to differences in bottom depths and circulation patterns at WBB stations (see Fig. 1B), for the purposes of this study, the area was considered distinct from BB itself.

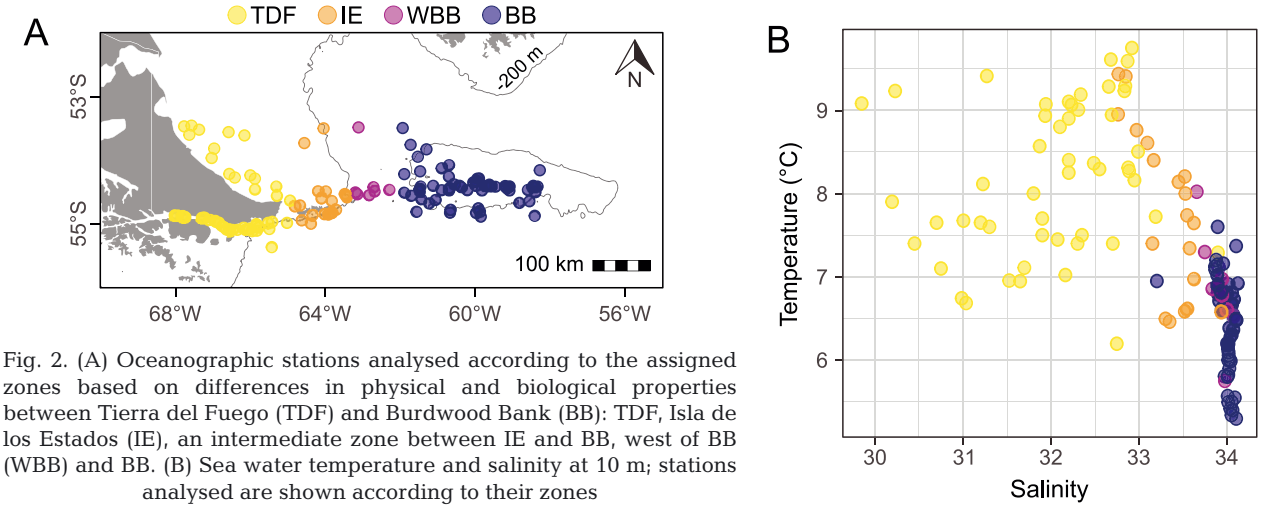

Fig. 2. (A) Oceanographic stations analysed according to the assigned zones based on differences in physical and biological properties between Tierra del Fuego (TDF) and Burdwood Bank (BB): TDF, Isla de los Estados (IE), an intermediate zone between IE and BB, west of BB (WBB) and BB. (B) Sea water temperature and salinity at 10 m; stations analysed are shown according to their zones

2.2. Sample processing

Fuegian sprats were sorted and identified using a Leica S6 D Greenough stereoscopic microscope. Eggs were recognized based on their spherical shape, the presence of a segmented yolk-sac, and the absence of an oil droplet (Ciechomski 1971). Four larval stages were identified based on the presence of a yolk-sac and the flexion degree of the notochord: yolk-sac, preflexion, flexion, and postflexion larvae (Kendall et al. 1984). Post-larval specimens were classified as metamorphosing (transitional larvae) or juvenile, the former presenting scales primarily in the ventral keel but with some body parts remaining transparent and the latter being totally covered in scales (Lebour 1921). Egg, larval, and post-larval abundances per station were standardized as density values (eggs m^{-2} or larvae and post-larvae per 100 m^3). Standard lengths (SL) of larval and post-larval sprats were measured from the tip of the snout to the end of the notochord to the nearest µm using a Carl Zeiss stereoscope equipped with Axio Vision software for the former, and to the nearest mm with a calliper for the latter. Shrinkage corrections were applied for sprats fixed in 80% alcohol and 4% formaldehyde following Fey (1999) and Petereit et al. (2008) for *Sprattus sprattus* larvae, respectively; no correction was required for frozen sprats (Petereit et al. 2008). Age and spawning dates were necessary to adjust the particle-tracking simulation protocols. This information was obtained from otolith microstructure analyses conducted on sagittae of sprats fixed in 80% alcohol or frozen. The analyses were restricted to sprats captured in TDF and BB. Details of the otolith extraction and daily increment measurement methodology are provided in García Alonso et al. (2020).

2.3. Data analysis

Statistical analyses and figures from empirical data and model results were carried out in R ver. 4.1.3 (R Core Team 2022). Figures were further edited in Inkscape™.

2.3.1. Spatiotemporal patterns of distribution and spawning estimates

The ontogenetic composition of larval and post-larval developmental stages of Fuegian sprats (expressed in percentages) was analysed for each zone and season. Data from the Bongo and IKMT nets employed in 2017 were pooled since no significant differences ($p = 0.12$) were found across their abundances when compared by means of linear models fitted by generalized least squares (heteroscedasticity was modelled with an 'identity' variance function and the level of significance used was 0.05).

Spawning dates were estimated for each habitat (TDF and BB) and cohort independently (2014–2015, 2015–2016, and 2016–2017) using SL and age data of specimens analysed. Spawning was assumed to occur 7 or 5 d prior to hatching for sprats from BB and TDF, respectively, based on *S. sprattus* reared at equivalent mean temperatures to those measured in both habitats (6 and 8°C) (Milligan 1986). The ages of yolk-sac larvae were set at 3 d, which is the maximum time for Fuegian sprat yolk-sac absorption (Leal et al. 2017). For larval and post-larval specimens with unanalysed otoliths, ages were back-calculated employing Von Bertalanffy growth models fitted to age–SL data, whereas a linear model was fitted for post-larval specimens (Fig. S1 in the Supplement at www.int-res.com/articles/suppl/m731p027_supp.pdf). Juvenile sprats were not included owing to insufficient observations (<5). Results were grouped by spawning month for each zone, differentiating the spawning frequencies (expressed in %) for each developmental stage.

2.3.2. Particle-tracking simulations

Passive particle-tracking simulations were used to identify drift, retention, and connectivity patterns from main spawning areas during peak spawning and compare them with those observed by empirical data. A Lagrangian particle-tracking algorithm was employed to compute the trajectories of passive particles based on the following equation:

$$\frac{dX}{dt} = A(X,t) + S_v(X,t) + S_h(X,t) \quad (1)$$

where X is the 3-dimensional (3D) position of the particle, t is the time, A is the advection term and S_v and S_h are sub-grid scale turbulent stochastic terms in the vertical and horizontal directions, respectively. The Lagrangian particle-tracking algorithm uses monthly averaged 3D velocities (A), and the vertical diffusivity coefficient (K_v) obtained from a high-resolution realistic hydrodynamic ocean model (see below). The formulation of the vertical stochastic term (S_v) is based on K_v.

The hydrodynamic model used in this study is a 3D, eddy-resolving, free surface, hydrostatic, primitive equation ocean model based on the Regional Ocean Modeling System (ROMS_AGRIF version; Debreu et al. 2012). The model domain covers an area from 58–38° S and from 69–51° W, with a horizontal resolution of 1/24° and 40 sigma levels in the vertical, and employs higher vertical resolution at the top and bottom layers (Matano et al. 2019). The bottom topography is derived from the ETOPO1 (1′ resolution) (Amante & Eakins 2009), which is smoothed to minimize pressure gradient errors associated with terrain-following coordinates. A combination of radiation and advection conditions is used at the open boundaries (Marchesiello et al. 2001). The model is forced with amplitudes and phases of the M_2 tide interpolated from a global TPXO6 tidal model (Egbert et al. 1994) as well as climatological values of temperature, salinity, and velocity fields from a larger model of the entire Southwestern Atlantic region with 1/12° horizontal resolution (Combes & Matano 2014). At the surface, the model is forced with the mean climatological wind stress derived from the 1999–2012 Quikscat-ASCAT climatology and heat, and freshwater fluxes derived from the Comprehensive Ocean–Atmosphere Data Set (Da Silva et al. 1994). Vertical mixing is parameterized with a K-Profile Parameterization scheme (Large et al. 1994) and bottom friction follows a quadratic formulation. This model has been successfully validated against empirical and satellite observations, reproducing key aspects of the regional circulation (Combes & Matano 2014, Matano et al. 2014, Strub et al. 2015, Combes & Matano 2018, 2019).

The sub-grid scale turbulence in the vertical direction (z), (S_v term in Eq. 1) is modelled through a random displacement model (Visser 1997) in the form:

$$\Delta z = \frac{\partial K_v(x,y,z,t)}{\partial z}\Delta t + \left[2r^{-1}K_v(x,y,z,t)\Delta t\right]^{1/2} R(t) \quad (2)$$

where Δz is the particle's (stochastic) vertical displacement, K_v is the vertical diffusion coefficient (provided by the hydrodynamic model), where x and y are the horizontal directions, z is the vertical direction and t is the time, R is a random process with zero mean and standard deviation r, and Δt is the stochastic time step.

We evaluated particle transport using monthly averaged climatological runs of the hydrodynamic model instead of year-specific forcing, owing to an insufficient number of stations and a lack of sampling areas to adequately assess year-specific variations. More importantly, empirical data showed strong seasonal variability in the abundance and distribution patterns of Fuegian sprat early life stages over several years (see Figs. 4–6). Thus, employing monthly averaged climatological runs emerged as the best approach to obtain a general overview of the use of spawning and nursery habitats by this species. Usually, studies using high-resolution circulation models consider the coefficient of horizontal diffusion (K_h) to be null in the simulations. Using monthly average velocities from a climatological run of a hydrodynamic model may overlook transient features, such as small eddies and other time-varying features of the circulation, possibly increasing the relevance of horizontal dispersion in the behaviour of passive particles. To account for horizontal turbulent mixing processes occurring at the sub-grid scale of the model, we conducted simulations using a simple model of horizontal sub-grid scale parameterization. This was achieved by implementing a Gaussian random flight process with additional horizontal displacements (Δx) in the form of a 'naive' random walk (Visser 1997):

$$\Delta x = R(t)\sqrt{2r^{-1}K_h\Delta t} \quad (3)$$

where R is a random process with zero mean and standard deviations r, and Δt is the stochastic time step. We estimated possible values of K_h for the study area using the Smagorinsky equation (Smagorinsky 1963) and the model's velocity fields. We selected 2 values different from 0 m s^{-2} (10 and 30 m s^{-2}) to evaluate the sensitivity of the analysis while covering a representative range of analytically estimated values of K_h (Fig. S2). The stochastic differential Eq. (1) was integrated using the Larval Transport Lagrangian Model (LTRANS, Schlag et al. 2008). LTRANS utilizes a sophisticated interpolation and smoothing scheme for the vertical diffusivity field K_v (tension splines), which preserves the monotonicity and convexity of the data field without adding inflection points. This ensures its compatibility for use in Eq. (2) and enables the simulation of horizontal turbulence using Eq. (3). Additional analyses were conducted for 2 austral springs (2014 and 2015) with and without horizontal diffusivity (K_h of 30 and 0 m s^{-2}, respectively) to investigate the model sensitivity by forcing it with daily wind data and using 5 d averaged velocity fields to feed the particle-tracking algorithm. These analyses confirmed that the monthly average circulation patterns correctly reproduced the dominant mode of variability with the values of K_h employed, even in a particularly complex area such as IE (Fig. S3).

Once the hydrodynamic model was defined and the K_h values were selected, we outlined the spatial and temporal strategy for the simulations (Fig. 3).

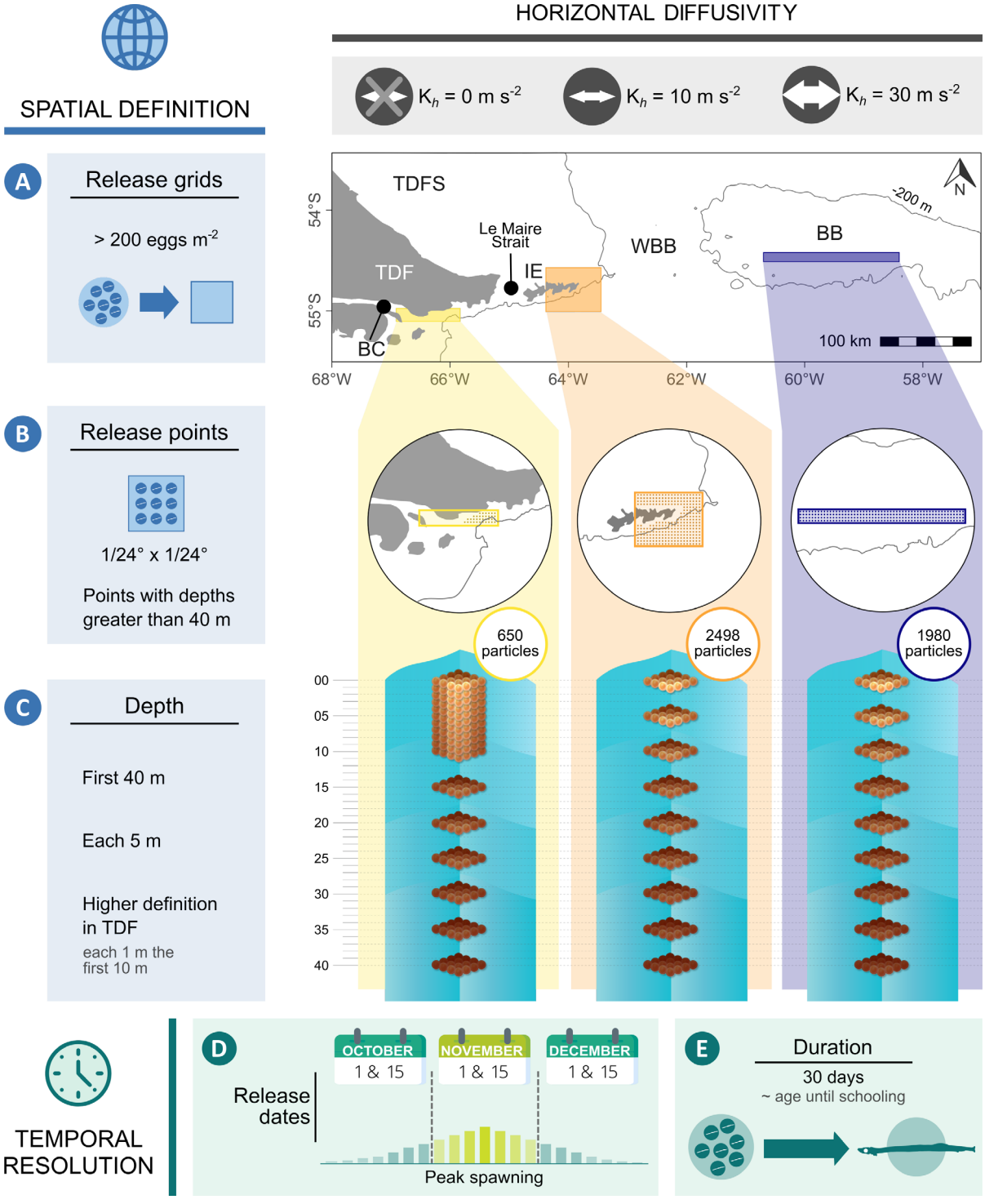

Fig. 3. Simulation strategy for particle-tracking of Fuegian sprat early life stages in the Southwest Atlantic Ocean without (K_h = 0 m s^{-2}) and with horizontal diffusivity in the model (K_h = 10 and 30 m s^{-2}) in austral spring. (A) Three release sites were selected and outlined based on egg abundances higher than 200 eggs m^{-2}: Tierra del Fuego (TDF), Isla de los Estados (IE), and Burdwood Bank (BB). (B) Particles within the grids were horizontally separated with a resolution of 1/24° and were only released from places with depths greater than 40 m. (C) Vertically, particles where released each 5 m within the first 40 m, except in TDF where a higher definition (1 m) was performed in the first 10 m. This resulted in 650, 2498, and 1980 particles released for TDF, IE, and BB, respectively. (D) A total of 6 dates of release were selected before, during, and after the spawning peak (1 and 15 October, November, and December), and (E) particles were tracked for 30 d after release (approximate age at which larvae could no longer be considered passive particles). BC: Beagle Channel; TDFS: Tierra del Fuego shelf; WBB: West Burdwood Bank

These were based on distribution, abundance, and estimated spawning dates of the Fuegian sprat. Spatially, the particle release grids were delimited based on stations where Fuegian sprat egg abundances were greater than 200 eggs m^{-2}, resulting in the configuration of 3 release grids: one in TDF (specifically in the BC) of 976 km^2, another in IE of 2900 km^2, and a third in BB of 1511 km^2. Particles within each grid were positioned with a horizontal resolution of 1/24° following the model's maximum resolution. Only particles located in areas with depths greater than 40 m were kept, to ensure the correct functioning of the model. Release positions located very close to the coastline in IE and the western section of the release grid in TDF were eliminated due to this methodological constraint. Vertically, particles were released in the first 40 m based on bibliographic references for the species in Chile (Landaeta et al. 2013, Contreras et al. 2014), with an interval of 5 m. A limited number of particles were released in TDF owing to a smaller release grid and the removal of several positions with depths shallower than 40 m. To balance the small number of particles released in TDF compared to IE and BB, a higher vertical definition was applied for the first 10 m depth in this release area, with particles released every 1 m. These additional release depths were set within the depth range already covered by the simulation to minimize possible differences in dispersal pathways. In total, 650 particles were released from TDF, 2498 particles from IE and 1980 particles from BB in each simulation. Temporally, particles were released every 15 d from 1 October to 15 December (a total of 6 release dates), covering the spawning peak observed in November (austral spring). Each particle was followed within a time window of 30 d. After this period, larvae are already in postflexion (the youngest larva in postflexion in our samples was 24 d old) and can no longer be considered passive particles since they acquire greater swimming capacity and tend to form schools, as seen for *S. sprattus* in the Northern Hemisphere (Peck et al. 2012b).

A total of 9 simulations were carried out, representing the 3 areas of release and the 3 values of K_h used. Particles that drifted vertically deeper than 200 m in the water column, representing 3.73–4.64 %, depending on the K_h value, were removed from further analyses. We evaluated the main patterns of transport by graphically depicting the final position of all particles released according to the release zones. Additionally, we assessed temporal and spatial variability by differentiating the final position of particles based on the release during austral spring (October, November, and December) and displaying the drift trajectories according to their depth (m). Areas of particle retention (closed gyres/vortices of particles) were visually identified in IE and BB during all simulations, being more readily apparent without horizontal diffusivity. These patterns are consistent with circulation vortices previously described for the area in the literature (e.g. Matano et al. 2019) and with the depth-average circulations patterns shown in Fig. S4. Percentages of retained particles were calculated across all simulations as the number of particles remaining in the identified areas divided by the total number of particles released in each zone. Overlapping particles from adjacent areas (TDF–IE and IE–BB) revealed connectivity between them. To assess the extent of connectivity, we generated polygons covering all particles for each zone, then calculated the overlapping areas among the polygons, and finally quantified connectivity as the percentage of particles in overlapping areas compared to the total number of particles released from the 2 areas considered (see Fig. A1 in the Appendix). retention and connectivity percentages were estimated considering both the final position of all particles (overall) and the month of release (October, November, and December) in austral spring.

Finally, we evaluated the agreement between empirical and modelled data for all values of K_h using a combination of graphical representations and quantitative tools. Empirical data used in this analysis included information from this study as well as studies conducted by Sánchez & Ciechomski (1995), Sánchez et al. (1997), and Ehrlich et al. (1999). Incorporating these references allowed us to expand the geographical extent of the results (which was limited by sampling designs) and, more importantly, to gain a general overview of the species' distribution. We selected stations sampled during austral spring and early summer, corresponding to the final date of the simulations and coinciding with the spatial extent of the particles. Only early larval abundances were considered, since the particles representing eggs were tracked for 30 d, after which they would have developed into early larvae. Polygons were constructed to delimit the final position of particles and the location of sampling stations, enabling us to assess the geographical correspondence and estimate the percentage of overlap between the 2 sources of information. Additionally, the longitudinal and latitudinal abundance modes of distribution of empirical and modelled data were evaluated through the construction of density curves.

3. RESULTS

3.1. Spatial and temporal patterns of distribution of the Fuegian sprat

Over 17 000 Fuegian sprat eggs were found in the samples analysed. Eggs were captured only during spring in all zones except the TDFS (Fig. 4). When present, egg abundances ranged from 7 to 2553 eggs m^{-2}. The maximum abundance was recorded at the centre of BB, although high abundances of over 200 eggs m^{-2} were also found at BC in TDF and IE.

In contrast to eggs, larval and post-larval sprats occurred in all seasons sampled (Fig. 5A). Their presence was continuous at BB but differed for the remaining habitats. During spring, sprats exhibited a similar distribution pattern to that of eggs, being found in all zones except in the TDFS. This was the season in which higher sprat abundances were registered overall, exhibiting mean abundances between 40 (WBB) and 286.53 ± 69.46 (TDF) larvae and post-larvae per 100 m^3, and with maximum abundances at the BC, IE and BB of 1446, 557, and 1128 larvae and post-larvae per 100 m^3, respectively. In summer, abundances did not surpass 20 larvae and post-larvae per 100 m^3; sprats were present in BB and IE but absent in the BC (TDFS and WBB were not sampled during this season). By autumn, sprats were only found at BB and TDF (primarily along the TDFS). Mean abundances ranged between 0.23 ± 0.12 and 1.12 ± 0.61 larvae and post-larvae per 100 m^3 for TDF and BB, respectively, with the maximum abundance of 28 larvae and post-larvae per 100 m^3 registered at BB. In the survey carried out closer to winter (autumn 2017), sprat larvae in BB were only captured at its western limit (see Fig. A2 in the Appendix).

Seasonal variability in larval and post-larval developmental stages was also observed across the study area (Fig. 5B). During spring, only early larvae (until flexion) were registered, with yolk-sac larvae being exclusively captured in this season. A clear dominance of preflexion larvae was observed in the eastern region of the study area (92% in the WBB and 65% at BB). Postflexion larvae were registered for the first time in summer at both IE and BB. However, as in spring, there was a dominance of more developed larvae in the east at BB (76%) compared to stations in the west at IE (29%). Significant differences were observed during autumn, when more than 90% of sprats found at BB were larvae in postflexion, with fewer flexion and preflexion larvae, whereas sprats found at TDF were mainly at a post-larval stage. Both metamorphosing and juvenile sprats comprised 57% of the sprats captured overall in this season, and postflexion larvae were the least developed stage found.

3.2. Spawning periods

Spawning dates were back-calculated from larvae and post-larvae captured at TDF and BB, showing the occurrence of a major peak during November at both sites, representing more than 50% of the total sprats analysed (Fig. 6). A more protracted spawning period was identified at BB from September to March; at TDF, spawning occurred between September and January. In terms of sprat developmental stages, most preflexion larvae were spawned during November, coinciding with the spawning peak observed in both zones. Differences between BB and TDF were also noted in the spawning period for the most developed stages. Metamorphosing sprats captured in TDF were spawned before or during the spawning peak whereas postflexion larvae were exclusively spawned after the peak. In contrast, postflexion larvae captured in BB were spawned throughout the spawning period, the majority spawning after the peak (in December and January).

3.3. Modelled transport, retention, and connectivity

Particles released in TDF (close to the mouth of the BC) in particle-tracking simulations without horizontal diffusivity (K_h = 0 m s^{-2}) were mostly transported north towards the TDFS through the Le Maire Strait, reaching about 54°S, with few particles drifting

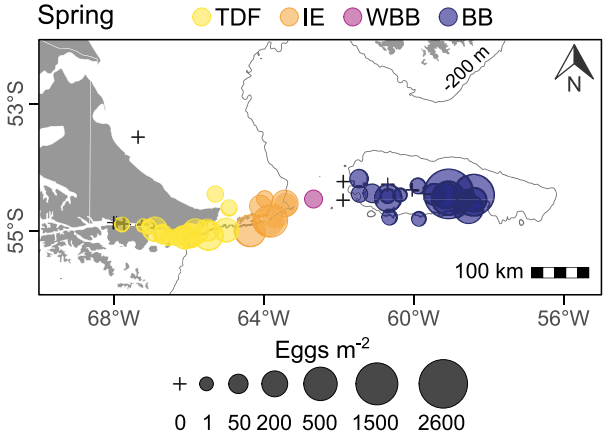

Fig. 4. Distribution and abundance of Fuegian sprat eggs throughout the study area in spring. TDF: Tierra del Fuego; IE: Isla de los Estados; WBB: West Burdwood Bank; BB: Burdwood Bank

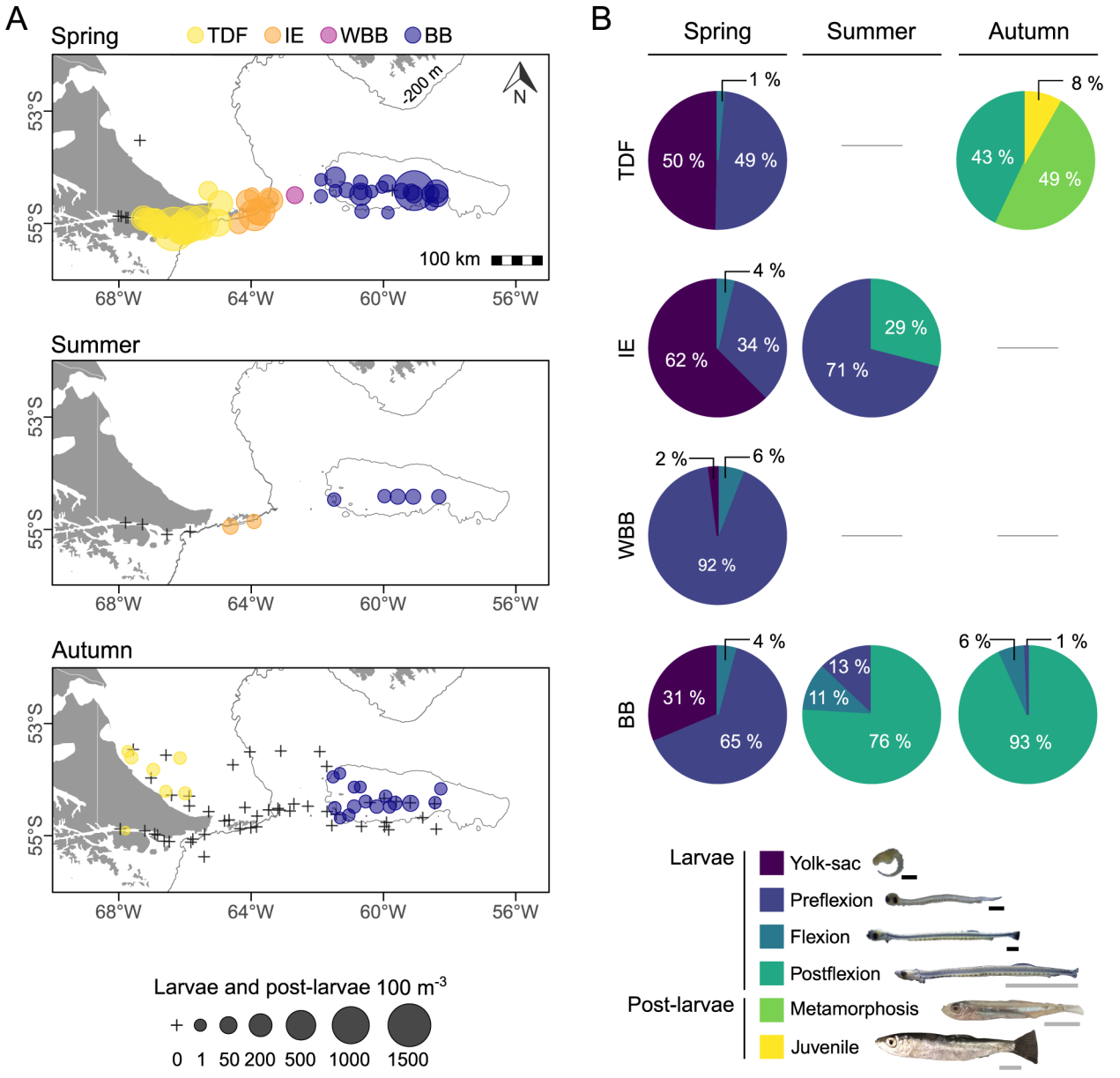

Fig. 5. (A) Seasonal distribution and abundance of Fuegian sprat in the study area and (B) ontogenetic composition according to the different developmental stages expressed in percentages. Horizontal lines represent the absence of sprat and/or sampling stations in specific zones and seasons. Scales below each sprat represent 1 mm (black lines) or 1 cm (grey lines). TDF: Tierra del Fuego; IE: Isla de los Estados; WBB: West Burdwood Bank; BB: Burdwood Bank

towards the east and reaching the southern coasts of IE (Fig. 7A). When released from BB, particles were transported towards the north and west of the bank, although nearly all particles remained within the 200 m isobath (over 99%). Particles released from IE showed the greatest dispersion, drifting east, west, and north of the release area, and reaching the northernmost distribution of all particles (approximately 53.5° S). Particles moving eastward covered the area identified as WBB between IE and BB, those moving north closely followed the 200 m isobath, and particles drifting towards the west intruded the continental shelf, reaching the middle of the TDFS.

Two different retention areas were identified: the most conspicuous, covering 5217 km^2, occurred at the centre of BB (approximately 59° W), and another of lesser extension (755 km^2) at the northeastern coast of IE. Overall, about 51 and 22% of particles released in BB and IE were retained in the mentioned areas, respectively (Table 2). Given the complex hydrodynamic setting in IE, particles were further differentiated into 3 release areas within the

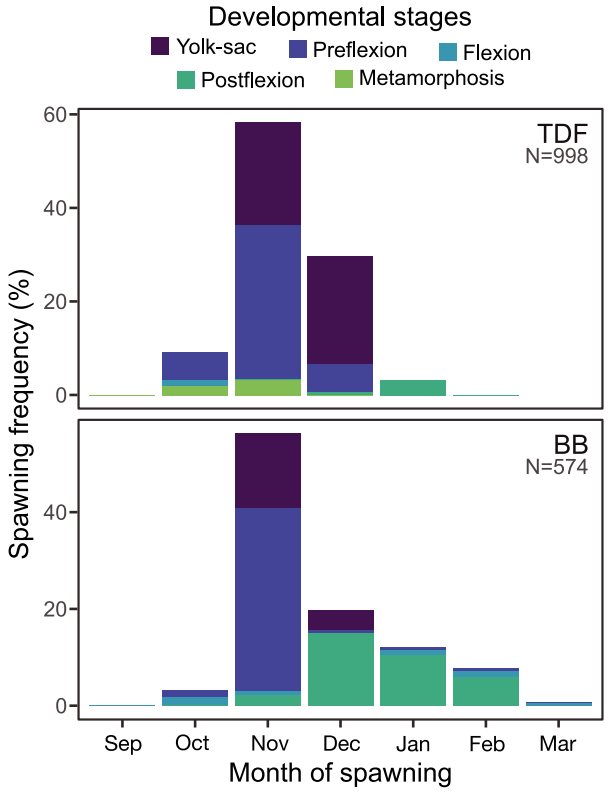

Fig. 6. Spawning frequencies of Fuegian sprat at Tiera del Fuego (TDF) and Burdwood Bank (BB) estimated by otolith microstructure analyses. Values per month are differentiated according to the developmental stages of the individuals analysed. N: number of sprats analysed for each zone

initial grid (south, east, and north of IE), revealing that retained particles were mainly those released north of the island (Fig. S5). Connectivity between neighbouring zones was observed between TDF and IE (mainly along the TDFS) and between IE and BB at the western limit of BB. Almost 28% of all particles released from TDF and IE overlapped over an extension of more than 4000 km^2, whereas the percentage of connectivity for IE and BB was less than 1% and occurred over a smaller area (684 km^2) (Table 3).

Table 2. Estimated retention of released particles in drift simulations at Isla de los Estados (IE) and Burdwood Bank (BB) in austral spring. Extensions of retention areas and retention values are shown considering overall results and according to the month of release for simulations with (K_h = 10 and 30 m s^{-2}) and without horizontal diffusivity (K_h = 0 m s^{-2})

Zone	Extension (km^2)	K_h (m s^{-2})	Retention (%) Total	Oct	Nov	Dec
IE	755	0	20.80	20.63	20.85	20.91
		10	18.17	18.22	18.00	18.29
		30	15.71	16.04	15.30	15.79
BB	5217	0	52.88	55.86	51.34	51.44
		10	52.36	55.35	50.83	50.88
		30	50.66	53.67	48.84	49.42

In terms of release month, particle drift pathways closely resembled the general patterns described above for all zones, with distances covered by particles markedly increasing from October to December (Fig. 7B–J). Only one exception to this trend was found: particles released from IE that drifted west (Fig. 7F) exhibited a larger westward displacement towards the middle of TDFS when released in November (during peak spawning) instead of December. Particle retention was identified at IE (Fig. 7C,F,I) and BB (Fig. 7D,G,J) regardless of the month of release. Retention percentages increased from October to December at IE, whereas the opposite appeared to occur for BB (Table 2). Connectivity between IE–TDF and IE–BB also increased from October to December. Particle overlap from different zones was first observed in December, with the highest percentage of connectivity seen for IE–TDF (Table 3).

Spatial patterns of particle trajectories considering horizontal diffusivity (K_h values of 10 and 30 m s^{-2}) were very similar to those previously described

Table 3. Estimated connectivity of released particles in drift simulations between Isla de los Estados (IE) and Tierra del Fuego (TDF), and IE and the Burdwood Bank (BB) in austral spring. Extensions of connectivity (Ext.) and connectivity (Conn.) values are shown considering overall results and according to the month of release for simulations with (K_h = 10 and 30 m s^{-2}) and without horizontal diffusivity (K_h = 0 m s^{-2}). Dashes represent zero connectivity

Zones	K_h (m s^{-2})	Total Ext. (km^2)	Total Conn. (%)	October Ext. (km^2)	October Conn. (%)	November Ext. (km^2)	November Conn. (%)	December Ext. (km^2)	December Conn. (%)
IE–TDF	0	4397	27.70	0	–	0	–	3705	29.10
	10	8579	37.09	0	–	1284	6.58	8055	36.22
	30	17038	56.54	288	3.11	5363	26.47	14811	41.85
IE–BB	0	684	0.46	0	–	0	–	684	0.84
	10	3415	3.90	0	–	27	0.01	3255	3.70
	30	6120	5.68	0	–	814	0.47	6025	5.50

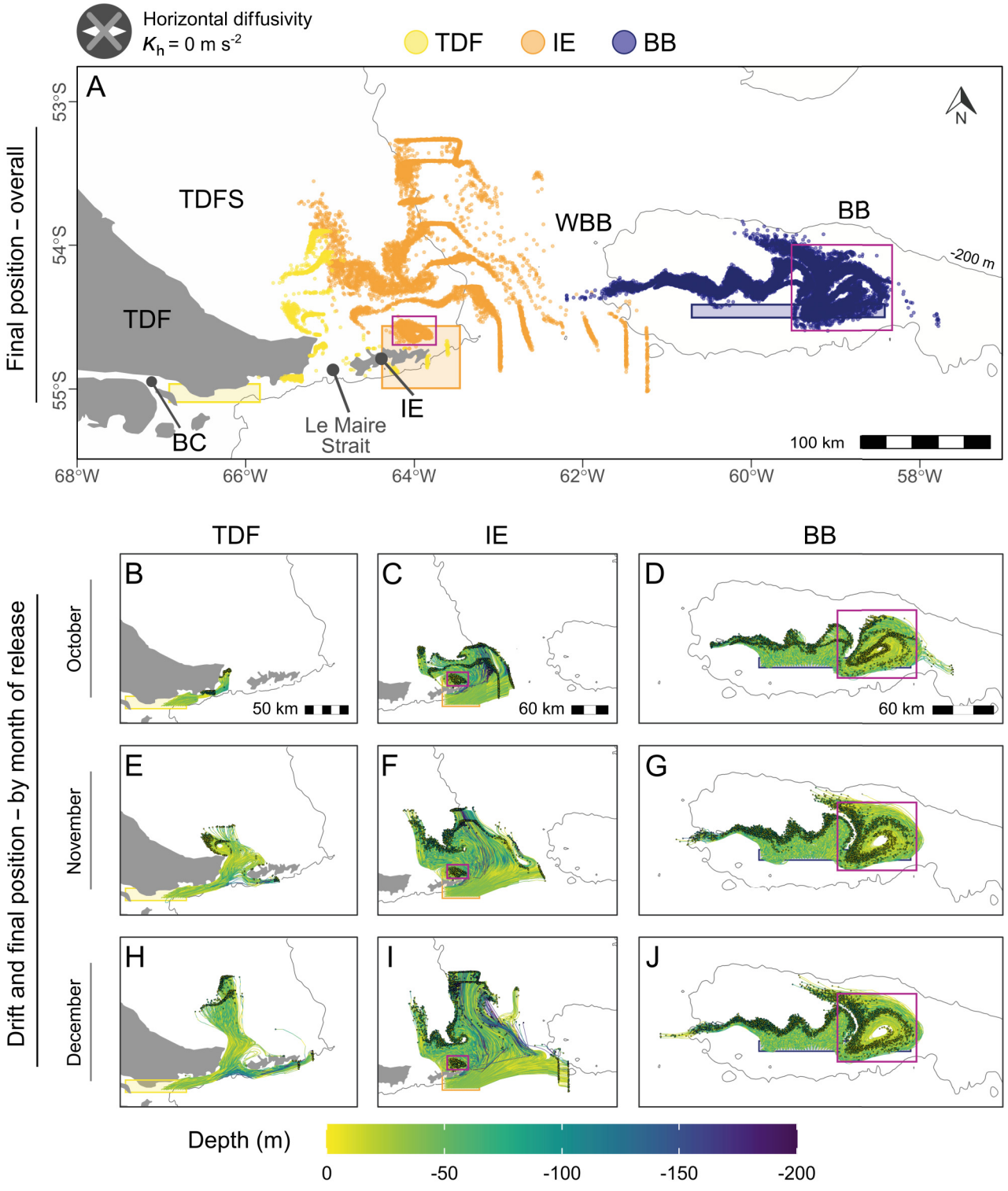

Fig. 7. Particle-tracking simulations without considering horizontal diffusivity (K_h = 0 m s^{-2}) in austral spring. (A) Final position (30 d after release) of all particles according to the zone of release. (B–J) Drift and final positions of the particles according to the month of release (October, November or December). Colours indicate the depth (m) of each particle during transport/retention. Release quadrants according to the release zones are indicated as filled rectangles. Pink rectangles in C-D, F-G, and I-J indicate recognised retention areas. TDF: Tierra del Fuego; BC: Beagle Channel; TDFS: Tierra del Fuego shelf; IE: Isla de los Estados; WBB: West Burdwood Bank; BB: Burdwood Bank

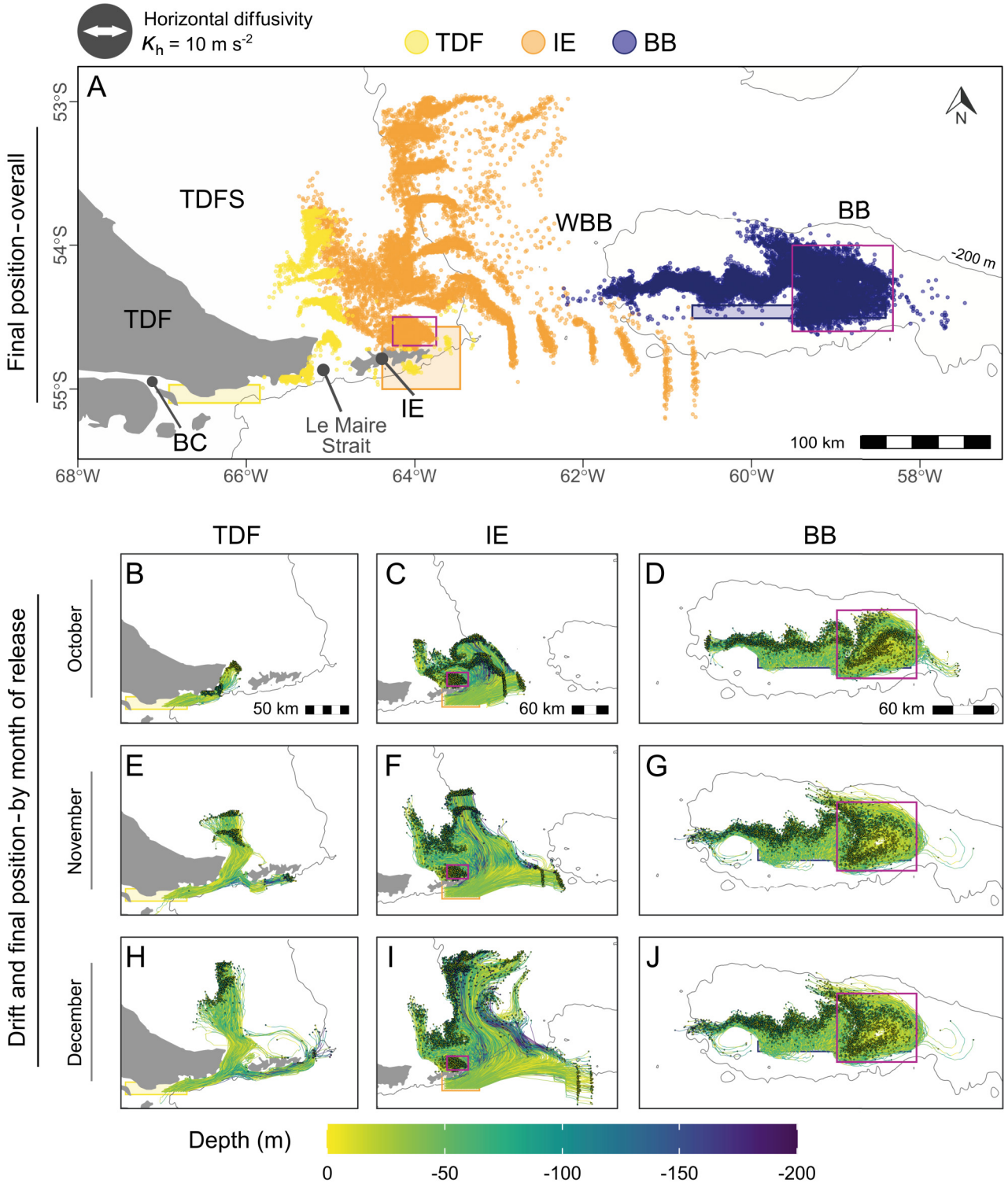

Fig. 8. As in Fig. 7, but for particle-tracking simulations considering horizontal diffusivity (K_h) of 10 m s^{-2}. Pink rectangles indicate retention areas recognised in simulations without considering horizontal diffusivity

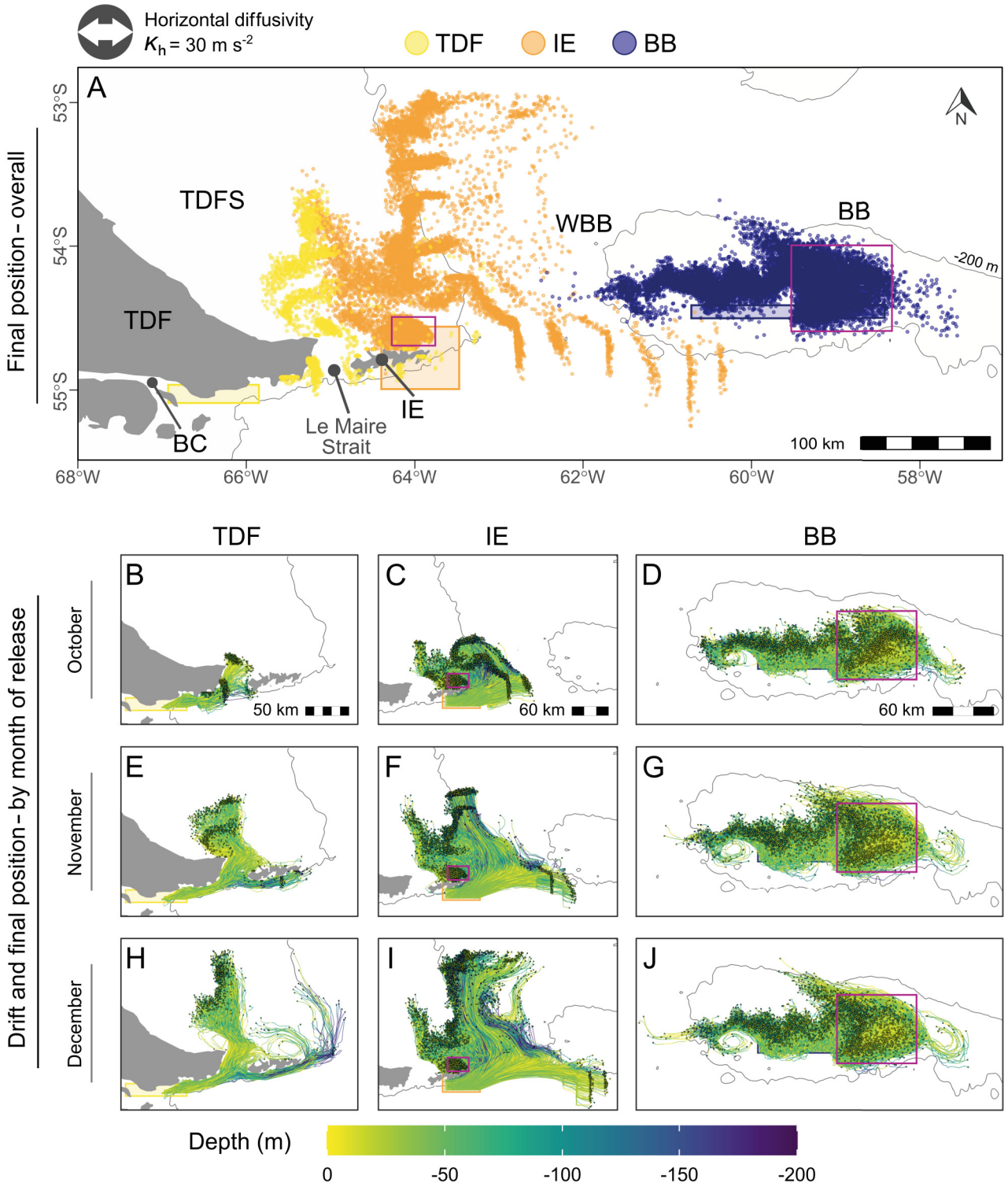

Fig. 9. As in Fig. 7, but for particle-tracking simulations considering horizontal diffusivity (K_h) of 30 m s^{-2}. Pink rectangles indicate retention areas recognised in simulations without considering horizontal diffusivity

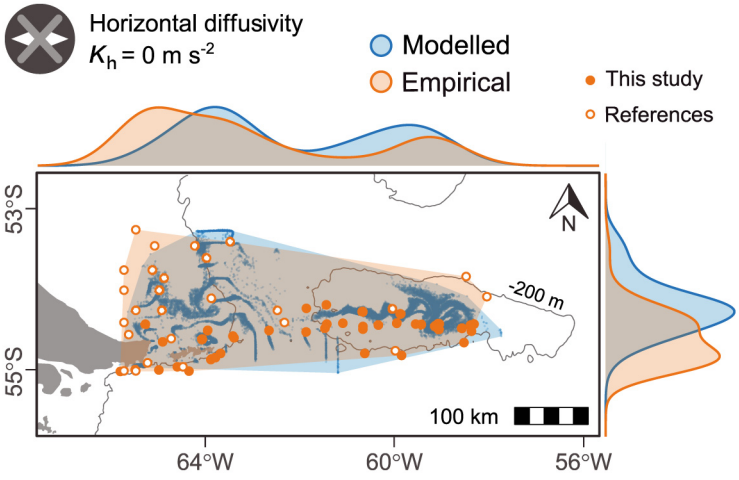

Fig. 10. Agreement between empirical and modelled data for simulations performed without considering horizontal diffusivity (K_h = 0 m s^{-2}). Circles on the map represent the particles' final positions (blue) and stations positive for Fuegian sprat early larvae sampled in austral spring and early summer (orange) during this (filled circles) and previous studies (empty circles). Density curves of longitudinal and latitudinal abundance distributions are shown at the top and right of the figure, respectively, for both types of data

(Figs. 8A & 9A). As expected, increasing the horizontal diffusivity resulted in greater dispersion of particles from all release zones and wider area coverage compared to the simulations performed with no diffusivity. Particles released from TDF reached northern latitudes (approximately 53.5° S) both inshore and along the shelf break. The connectivity of particles released from IE and TDF extended over a broader area between 8579 and 17038 km^2 and involved 37–57% of the total particles released from both zones for simulation with K_h values of 10 and 30 m s^{-2}, respectively (Table 3). Similarly, particles released from IE were further transported in all directions, with particles drifting east following the southern edge of BB and some entering the 200 m isobath. Most particles (99%) released from BB remained within the 200 m isobath but those outside this limit were further transported west and north of the bank. Overall, displacements increased from October to December, the months during which particles were released (Figs. 8B–J & 9B–J), with the exception of particles moving west from IE, which again intruded further into the TDFS when released in November (Figs. 8F & 9F). Only a relatively small number of particles released from IE reached the southern border of BB (Figs. 8F,I & 9F,I). The percentage of retention was estimated for the same areas identified in Fig. 7. Retention decreased in both areas with respect to simulations without considering horizontal diffusivity; however, this decrease represented less than 5% in all cases considered (Table 2).

Stations positive for early larvae during austral spring and early summer from this and previous studies coincided spatially with particles released in simulations performed without considering horizontal diffusivity (over 90%; Fig. 10). Empirical and modelled data also exhibited similar density distributions, both longitudinally and latitudinally, which largely overlapped. A bimodal shape was readily apparent longitudinally, with coinciding peaks at the centre of BB and at IE. In contrast, latitudinally, the distribution was unimodal, with both peaks occurring close to 54° S but with a slight displacement to the north in the case of modelled data. In a similar manner, in simulations considering horizontal diffusivity (Fig. S6), polygons presented a large overlap (85.7 and 84.3% for K_h values of 10 and 30 m s^{-2}, respectively). Density curves exhibited modes of abundance coinciding with those described previously, with abundance distributions showing greater overlap than when horizontal diffusivity was not considered.

4. DISCUSSION

To our knowledge, the present study is the first to both (1) simultaneously address the spatiotemporal distribution of Fuegian sprat early life stages along multiple habitats of the SWAO, and (2) conduct particle-tracking simulations based on empirical data for the Fuegian sprat (and planktonic organisms overall) from the southern SWAO. The good agreement between empirical and modelled data has allowed us to integrate the data from the 2 sources, providing a more comprehensive scheme of the dynamics of Fuegian sprat early life stages at their southernmost distribution, though some of the dispersal pathways remain in the realm of the hypothetical (Fig. 11). Overall, the analysed patterns of distribution and abundance reveal strong seasonal variability and a dominant influence of major circulation patterns in their dynamics. These findings not only constitute a much-needed update on Fuegian sprat biology, but also bring to light novel aspects of spawning activity

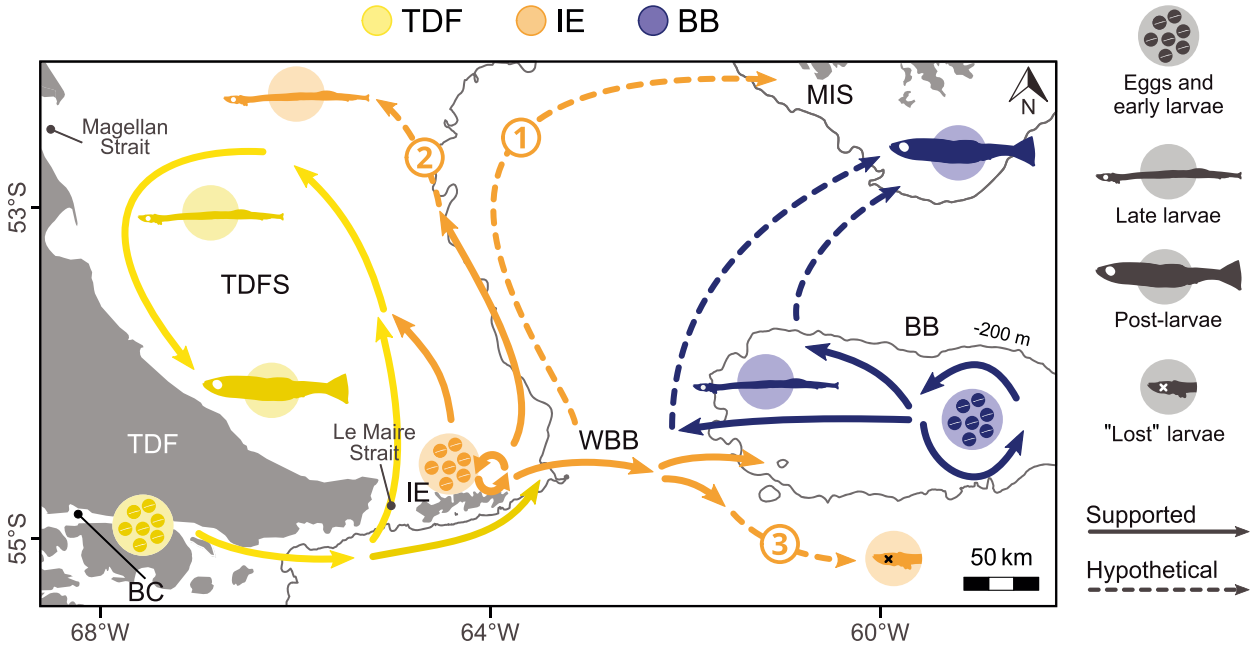

Fig. 11. Schematic representation of dispersal patterns of Fuegian sprat early life stages between Tierra del Fuego (TDF) and the Burdwood Bank (BB) showing dispersal routes supported by both empirical and modelled data (solid arrows) together with hypothetical pathways (dashed arrows). BC: Beagle Channel; TDFS: Tierra del Fuego shelf; IE: Isla de los Estados; WBB: West Burdwood Bank; BB: Burdwood Bank: MIS: Malvinas Islands Shelf

and connectivity across habitats, highlighting particle-tracking models as a suitable methodology for the assessment of Fuegian sprat recruitment in particular, and the dispersal of planktonic organisms in general.

One of the main outcomes of this study is the finding of Fuegian sprat eggs and early larvae along the entire area between TDF and BB in spring across all surveys, highlighting this region as a key domain for sprat reproduction in the SWAO. Although the use of different gear in the spring survey of 2015 probably undermined sprat abundances, distribution patterns and high abundances were consistent across surveys, further supporting our findings. Spawning and early nursery areas were previously reported at TDF and BB (Sánchez & Ciechomski 1995, García Alonso et al. 2018). However, this is the first time that eggs have been found at IE, and in high abundance, suggesting that IE probably operates as a third spawning ground for Fuegian sprats in the SWAO. Selection of a specific site within a spawning habitat appears to be related to the presence of adequate feeding conditions for adults of marine clupeids, the most intense spawning for some species often occurring in frontal areas (Blaxter & Hunter 1982). The latter could be the case for IE, which presents a frontal area along the 200 m isobath south and east of the island (Acha et al. 2004), although adequate food supply could also be a determining factor (Cepeda et al. 2018, Spinelli et al. 2020). There is still no clear explanation for the selection of IE as a spawning site by Fuegian sprats, nor is it known whether adults that spawn in IE are part of an established population or a separate one. So far, only 2 Fuegian sprat populations are recognized: one inhabits the Patagonian coasts of the SPS and the other the Malvinas Islands (Casarsa et al. 2019). The Patagonian population is more likely to spawn at IE given the geographical proximity and shared hydrodynamic features (Palma et al. 2021).

Eggs and early larvae found in WBB were less abundant compared to those in other areas. This finding, coupled with the fact that Fuegian sprats inhabit shallower coastal waters (Whitehead 1985a), suggests that eggs and early larvae are transported to the WBB rather than being spawned there. Considering the dispersal pathways and the number of particles drifting from IE to the WBB in the simulations (which increased when horizontal diffusivity was considered in the model), it is likely that the sprats found at WBB might originate in IE. However, the high percentage of preflexion larvae found in WBB in spring is more similar to the developmental composition of sprats found at BB, which also showed particle transport towards the WBB in the simulations. Backward simulations could help identify the most likely source (Torrado et al. 2021), although

LTRANS does not provide this tool and we lack sufficient data to validate potential origins (due to the absence of sampling stations in certain locations and limitations posed by the resolution of the hydrodynamic model). Previous simulations with the same hydrodynamical model and a different particle-tracking software allowing backtracking (Batchelder 2006) did show some connectivity between WBB and the southward portion of IE (Matano et al. 2019), supporting the hypothesis that IE would be the main source for sprats found at WBB. Interestingly, backward and forward simulations have also shown some connectivity between WBB and the Malvinas Islands Shelf (Palma et al. 2021). Thus, sprats at WBB might be transported to the Malvinas Islands Shelf following the main currents of the Malvinas embayment (dashed orange arrow number 1 in Fig. 11), although it is yet to be confirmed whether this is the case and if early larvae endure such strong currents.

Despite the role of IE as a spawning ground, the lack of larvae during autumn suggests that only TDF and BB would be suitable nursery grounds for postflexion sprats. Fishes with pelagic eggs often reproduce in productive gyres to secure larval feeding success and/or prevent offshore dispersal (Loeb 1980). TDF and BB both present oceanographic features such as these, with anticyclonic gyres occurring in the TDFS and around the rim of BB (Palma et al. 2008, Matano et al. 2019; see Fig. 1B). These circulation patterns were replicated by both empirical and modelled data of Fuegian sprat distribution at TDF and BB, corroborating a high degree of resemblance between the findings of the 2 methodologies. Overall, eggs and early larvae are transported from the BC towards the TDFS in TDF (solid yellow arrows in Fig. 11), whereas in BB they are mainly retained at the centre, although some transport towards the north and west is also evident within the bank (solid violet arrows in Fig. 11). These patterns are consistent with those found in previous studies (Sánchez et al. 1995, García Alonso et al. 2018) and suggest that recruitment success is likely coupled to main ocean currents transporting or retaining larvae (Hjort 1914, Iles & Sinclair 1982), as observed with other clupeids (Ospina-Alvarez et al. 2015). Further studies addressing Fuegian sprat recruitment success are required to verify these hypotheses.

In addition to the differing recruitment processes operating at TDF and BB, a further disparity was the presence of post-larval sprats (metamorphosing and juveniles) in the former location and absence in the latter. Slower growth associated with lower temperatures at BB (García Alonso et al. 2020) could explain this finding, with post-larvae occurring there later in the year (probably in winter, the subsequent season). However, sprats are known to approach coastal nursery grounds during winter (Whitehead 1985b), which could also account for their absence in BB. Recent particle-tracking simulations using the same hydrodynamical model show a connection between the northern and western limits of BB with the Malvinas Islands Shelf, particularly in spring (Matano et al. 2019, Palma et al. 2021). Our simulations indicate that larvae released at BB are transported towards these areas, a pattern supported by empirical data; sprat larvae have been found north of BB and south of the Malvinas Islands (areas not included in our surveys) in the same survey by Ciechomski et al. (1975), and across the entire extent of BB in all the surveys analysed in this study. Specifically, sprat larvae found in the survey closest to winter were only present in the western section (see Fig. A2) and happen to be the oldest sprat larvae sampled. Given that there is a recognized Fuegian sprat population at Malvinas Islands (Cousseau 1982, Casarsa et al. 2019), their proximity to BB and similar hydrographic context could indicate that postflexion sprats take advantage of the regional circulation (Matano et al. 2019, Palma et al. 2021) and migrate towards the Malvinas Islands Shelf (dashed violet arrows in Fig. 11). If so, sprats spawned at BB could potentially mix with the Malvinas Islands population.

The absence of larvae at IE in autumn was unexpected, given the identification of a persistent retention area in all simulations in the northwestern region of the island. Most particles released from IE were transported rather than being retained (the maximum retention was under 21%), which could explain the absence of late larvae in the area. This finding is in consonance with the strong currents surrounding IE to the west (through Le Maire Strait) and to the east (an ACC branch) (Palma et al. 2021). Future studies will be required to explore whether other biological factors influencing larval development and/or survival (e.g. food supply, predation) could account for this outcome. Despite the absence of Fuegian sprat at IE in autumn, this spawning location appears to play a key role in supplying early life stages to adjacent areas. According to our simulations, eggs and early larvae spawned at IE and dispersed to the west overlap with those spawned in the BC at the TDFS, possibly merging with the TDF population. This relationship is also supported by the high degree of connectivity between TDF and IE (close to 57% overall). Although connectivity estimates indicate that particles released in December

exhibit the highest connectivity between these sites, particle intrusion from IE towards the TDFS was greater during peak spawning in November, underscoring the considerable connectivity among different habitats. Population persistence is fundamentally linked to rates of larval delivery and recruitment, and thus also connectivity among subpopulations (Cowen & Sponaugle 2009). The connectivity between IE and TDF could, therefore, have crucial biological consequences for the Patagonian sprat inhabiting the SPS. Further analysis involving adult populations is required to corroborate whether these larvae grow and spawn successive generations in TDF, or whether they return to IE, making this a case of post-spawning overlap rather than population connectivity.

Our simulation results also suggest a hypothetical connection between sprat dispersed north of IE and the Patagonian population (dashed orange arrow number 2 in Fig. 11). Particles drifting north followed the 200 m isobath delimiting the shelf break, known to be a highly productive environment (Acha et al. 2004). Larvae transported onshore or near the shelf break in this frontal system could benefit from adequate food supply, as evidenced by higher growth rates (García Alonso et al. 2020), and possibly increase their survival potential, as seen for *Sprattus sprattus* (Daewel et al. 2008). Besides constituting additional prey for commercially exploited fishes (e.g. Alvarez et al. 2022) in this area of intense fishing (Vasconcellos & Csirke 2011; Fig. S7), sprat larvae transported north could reach coastal zones near the Magellan Strait and further north along the SPS, where post-larval and juvenile Fuegian sprats are known to occur (Sánchez et al. 1995). Although spawning activity has not been thoroughly analysed north of the study area, spawning likely occurs also within the Magellan Strait, possibly contributing to the Patagonian population and further increasing connectivity among potential subpopulations. Broadening the temporal and/or spatial extension of particle-tracking simulations could be useful in further addressing this issue.

Particles released from IE that drifted towards the WBB or along the southwestern edge of BB exhibited some unusual linear patterns, especially evident in simulations carried out without horizontal diffusivity. We identified these patterns as artefacts of the rectangular-shaped release grids; the strong eastward transport of the ACC in the area advects particles in the original linear boundary of the release area almost at the same speed, consequently generating the observed linear patterns. Employing different shapes of releasing grids such as Gaussian ellipsoids or other methodological strategies (such as releasing particles corresponding in number or statistical weight to the observed egg abundances per station) could prevent this methodological artefact, offering additional insight into Fuegian sprat distribution pathways. Despite the peculiarity of the pattern described, it is important to highlight that the early larvae transported to the WBB and the southern edge of BB arrive at less productive oceanic areas subject to intense currents, reducing the survival probability of the larvae. Hence, these larvae can be regarded as 'lost' (dashed orange arrow number 3 in Fig. 11), not contributing significantly to the functioning populations (Parrish et al. 1981).

There are certain intrinsic limitations to our data and methodological approach, such as the 40 m cut-off in particle release locations (which hampered simulations from the inner section of the BC in TDF), and the restricted temporal and geographical extent of the empirical information gathered in our study compared to modelled distributions, among others. Notwithstanding these limitations, our simulations show clear signs of early-stage drift and retention pathways in good agreement with empirical data from this and previous studies (Sánchez & Ciechomski 1995, Sánchez et al. 1997, Ehrlich et al. 1999), further corroborating the temporal and spatial robustness of modelled results compared to empirical data on the species. As more information becomes available, future studies will likely address still unresolved questions relating to population connectivity and recruitment success. To this end, it would be useful to study the biological traits of surviving individuals, such as their growth, since relying solely on average values of larval traits may misrepresent the proportion of larvae successfully contributing to population connectivity (Chaput et al. 2022). Moreover, fish larval drift can exhibit strong interannual variability related to wider climate variability in dispersal trajectories such as wind patterns and main currents (Suca et al. 2022) or mesoscale eddies (Ospina-Alvarez et al. 2015). Based on our findings, sampling strategies of future studies should include stations in TDFS, BB, and, if possible, the Malvinas Islands Shelf across multiple years to successfully retrieve signs of shifts in Fuegian sprat patterns of distribution.

The lack of commercial extraction and economic stimulus has relegated efforts towards a better understanding of the biology of the Fuegian sprat in the SWAO. Nevertheless, the different habitats and oceanographic currents occurring between TDF and BB offer a unique opportunity to assess the distribution of early stages of the species and

undertake environmental modulation in a natural scenario. These factors also enabled connectivity patterns among adjacent spawning areas to be identified, of crucial relevance for evaluating and designing Marine Protected Area networks in the region, such as those proposed under the national 'Pampa Azul' initiative; it is through this type of analysis that effective management practices emerge (Ospina-Alvarez et al. 2020). This is especially relevant for small pelagic fishes, which can show extreme fluctuations in their biomass even in the absence of harvesting pressure (Lasker 1978). Identifying underlying drivers and processes modulating the recruitment of foundation species like the Fuegian sprat is of paramount importance in avoiding possible detrimental economic and ecologic consequences. In this sense, dispersal simulations provide a powerful tool that can be used to corroborate predator distribution in association with the drift of their larval prey (Sandvik et al. 2016). This baseline information can be of crucial value in assessing possible shifts induced by climate change in the distribution of fish and their associated predators, as reported for other species in the SWAO (Franco et al. 2020) and other regions around the world (Perry et al. 2005, Petitgas et al. 2012, Campana et al. 2020).

Data availability. Source code and packages employed are available at https://github.com/virginiagarciaalonso/fuegian_sprat_ELS.

Acknowledgements. This study was supported by the Consejo Nacional de Investigaciones Científicas y Técnicas (CONICET), Argentina (PIP 11220150100109CO 2015-2017), the Universidad de Buenos Aires, Argentina (UBACYT 20020190100133BA 2020-2024), and the Pampa Azul Interministerial Initiative implemented by the Argentinian Ministry for Science, Technology and Productive Innovation. E.D.P. acknowledges financial support from Agencia Nacional de Promoción Científica y Tecnológica (grant PICT-2020-02024) and Universidad Nacional del Sur (grant 24F079), Argentina. The authors thank Luciano Padovani, Alejandro Martinez, and everyone who participated in the oceanographic surveys for their cooperation during sample collection and preparation, Pablo S. Milla Carmona for his statistical advice and Denise Attadia for her collaboration in the design of Fig. 3. The authors also thank the editor Alejandro Gallego, and the reviewers T. Dobbelaere, J. J. Suca, and an anonymous referee for their insights and valuable suggestions. This is INIDEP contribution No. 2298 and Marine Protected Area Namuncurá-Burdwood Bank (Law 26,875) contribution No. 71. This publication is based upon work from COST Action Unifying Approaches to Marine Connectivity for Improved Resource Management for the Seas (SEA-UNICORN) CA19107, supported by COST (European Cooperation in Science and Technology, www.cost.eu).

LITERATURE CITED

Acevedo J, Urbán J (2021) Estimates of Fuegian sprat consumption by humpback whales in the Magellan Strait feeding area as predicted by a bioenergetic model. Mar Ecol Prog Ser 657:223–239

Acha EM, Mianzan HW, Guerrero RA, Favero M, Bava J (2004) Marine fronts at the continental shelves of austral South America: physical and ecological processes. J Mar Syst 44:83–105

Alheit J, Hagen E (2001) The effect of climatic variation on pelagic fish and fisheries. In: Jones PD, Ogilvie AEJ, Davies TD, Briffa KR (eds) History and climate. Springer, Boston, MA, p 247–265

Alvarez CD, Giussi AR, Botto F (2022) Trophic variability of long tail hake *Macruronus magellanicus* in the Southwestern Atlantic: movements evidenced by stomach content and stable isotope analysis. Polar Biol 45:1131–1143

Amante C, Eakins BW (2009) ETOPO1 1 Arc-minute global relief model: procedures, data sources and analysis. NOAA Tech Memo NESDIS NDGC-24. National Geophysical Data Center, Boulder, CO

Balestrini C, Manzella G, Lovrich GA (1998) Simulación de corrientes en el Canal Beagle y Bahía Ushuaia, mediante un modelo bidimensional. Informe técnico no. 98. Departamento de Oceanografía, Buenos Aires

Batchelder HP (2006) Forward-in-time-/backward-in-time-trajectory (FITT/BITT) modeling of particles and organisms in the coastal ocean. J Atmos Ocean Technol 23: 727–741

Baudron AR, Brunel T, Blanchet MA, Hidalgo M and others (2020) Changing fish distributions challenge the effective management of European fisheries. Ecography 43: 494–505

Baumann H, Hinrichsen HH, Möllmann C, Köster FW, Malzahn AM, Temming A (2006a) Recruitment variability in Baltic Sea sprat (*Sprattus sprattus*) is tightly coupled to temperature and transport patterns affecting the larval and early juvenile stages. Can J Fish Aquat Sci 63: 2191–2201

Baumann H, Hinrichsen HH, Voss R, Stepputtis D, Grygiel W, Clausen LW, Temming A (2006b) Linking growth to environmental histories in central Baltic young-of-the-year sprat, *Sprattus sprattus*: an approach based on otolith microstructure analysis and hydrodynamic modelling. Fish Oceanogr 15:465–476

Bellisio NB, López RB, Torno A (1979) Peces marinos patagónicos. Secretaria de Estado de Intereses Marítimos, Subsecretaría de Pesca, Buenos Aires

Blaxter JHS, Hunter JR (1982) The biology of the clupeoid fishes. Adv Mar Biol 20:1–223

Brun AA, Ramirez N, Pizarro O, Piola AR (2020) The role of the Magellan Strait on the southwest South Atlantic shelf. Estuar Coast Shelf Sci 237:106661

Campana SE, Stefánsdóttir RB, Jakobsdóttir K, Sólmundsson J (2020) Shifting fish distributions in warming sub-Arctic oceans. Sci Rep 10:16448

Casarsa L, Diez MJ, Madirolas A, Cabreira AG, Buratti CC (2019) Morphometric description of schools from two different stocks of the southernmost sprat *Sprattus fuegensis.* Fish Res 212:29–34

Cepeda GD, Temperoni B, Sabatini ME, Viñas MD and others (2018) Zooplankton communities of the Argentine Continental Shelf (SW Atlantic, ca. 34°–55°S), an overview. In: Hoffmeyer M, Sabatini M, Bryini F, Calliari D, Santinell

N (eds) Plankton ecology of the Southwestern Atlantic. Springer International Publishing, Cham, p 171–199
Cerna F, Leal E, López A, Plaza G (2014) Age, growth and natural mortality of the Patagonian sprat *Sprattus fuegensis* (Jenyns, 1842) in Chiloé inland sea, southern Chile. Lat Am J Aquat Res 42:580–587
Chaput R, Sochala P, Miron P, Kourafalou VH, Iskandarani M (2022) Quantitative uncertainty estimation in biophysical models of fish larval connectivity in the Florida Keys. ICES J Mar Sci 79:609–632
Ciechomski JD (1971) Estudio sobre los huevos y larvas de la sardina fueguina *Sprattus fuegensis* y de *Maurolicus muelleri*, hallados en aguas adyacentes al sector patagónico argentino. Physis 30:557–567
Ciechomski JD, Cassia MC, Weiss G (1975) Distribución de huevos, larvas y juveniles de peces en los sectores surbonaerenses, patagónico y fueguino del Mar Epicontinental Argentino en relación con las condiciones ambientales, en noviembre 1973-enero 1974. Ecosur 2:219–248
Combes V, Matano RP (2014) A two-way nested simulation of the oceanic circulation in the Southwestern Atlantic. J Geophys Res Oceans 119:731–756
Combes V, Matano RP (2018) The Patagonian shelf circulation: drivers and variability. Prog Oceanogr 167:24–43
Combes V, Matano RP (2019) On the origins of the low-frequency sea surface height variability of the Patagonia shelf region. Ocean Model 142:101454
Contreras T, Castro LR, Montecinos S, Gonzalez HE, Soto S, Muñoz MI, Palma S (2014) Environmental conditions, early life stages distributions and larval feeding of Patagonian sprat *Sprattus fuegensis* and common sardine *Strangomera bentincki* in fjords and channels of the northern Chilean Patagonia. Prog Oceanogr 129: 136–148
Cousseau MB (1982) Revisión taxonómica y análisis de los caracteres morfométricos y merísticos de la sardina fueguina, *Sprattus fuegensis* (Jenyns, 1842) (Pisces, Clupeidae). Rev Invest Desarr Pesq 3:77–94
Cowen RK, Sponaugle S (2009) Larval dispersal and marine population connectivity. Annu Rev Mar Sci 1:443–466
Cury P, Bakun A, Crawford RJ, Jarre A, Quinones RA, Shannon LJ, Verheye HM (2000) Small pelagics in upwelling systems: patterns of interaction and structural changes in 'wasp-waist' ecosystems. ICES J Mar Sci 57:603–618
Da Silva AM, Young CC, Levitus S (1994) Atlas of surface marine data 1994, Vol 1: algorithms and procedures. NOAA Atlas NESDIS 6:20910-3282
Daewel UTE, Peck MA, Kuehn W, John MAST, Alekseeva I, Schrum C (2008) Coupling ecosystem and individual-based models to simulate the influence of environmental variability on potential growth and survival of larval sprat (*Sprattus sprattus* L.) in the North Sea. Fish Oceanogr 17:333–351
Debreu L, Marchesiello P, Penven P, Cambon G (2012) Two-way nesting in split-explicit ocean models: algorithms, implementation and validation. Ocean Model 49–50: 1–21
Egbert GD, Bennett AF, Foreman MG (1994) TOPEX/POSEIDON tides estimated using a global inverse model. J Geophys Res C Oceans 99:24821–24852
Ehrlich MD, Sánchez RP, De Ciechomski JD, Machinandiarena L, Pájaro M (1999) Ichthyoplankton composition, distribution and abundance on the southern Patagonian shelf and adjacent waters. INIDEP Doc Cient 5:37–65
FAO (2020) The state of world fisheries and aquaculture 2020. Sustainability in action. FAO, Rome
Fey DP (1999) Effects of preservation technique on the length of larval fish: methods of correcting estimates and their implication for studying growth rates. Arch Fish Mar Res 47:17–29
Fey DP (2015) Size and growth rate differences of larval Baltic sprat *Sprattus sprattus* collected with Bongo and MIK nets. J Fish Biol 86:355–359
Franco BC, Defeo O, Piola AR, Barreiro M and others (2020) Climate change impacts on the atmospheric circulation, ocean, and fisheries in the southwest South Atlantic Ocean: a review. Clim Change 162:2359–2377
García Alonso VA, Brown D, Martín J, Pájaro M, Capitanio FL (2018) Seasonal patterns of Patagonian sprat *Sprattus fuegensis* early life stages in an open sea sub-Antarctic Marine Protected Area. Polar Biol 41:2167–2179
García Alonso VA, Brown DR, Pájaro M, Capitanio FL (2020) Growing up down south: spatial and temporal variability in early growth of Fuegian sprat *Sprattus fuegensis* from the Southwest Atlantic Ocean. Front Mar Sci 7:322
García Alonso VA, Diaz MV, Pájaro M, Capitanio FL (2021) Ontogeny versus environmental forcing off the Southwest Atlantic Ocean: nutritional condition of Fuegian sprat *Sprattus fuegensis* early stages. Fish Oceanogr 30: 653–665
Guerrero RA, Baldoni AG, Benavides HR (1999) Oceanographic conditions at the southern end of the Argentine continental slope. INIDEP Doc Cient 5:7–22
Guihou K, Piola AR, Palma ED, Chidichimo MP (2020) Dynamical connections between large marine ecosystems of austral South America based on numerical simulations. Ocean Sci 16:271–290
Hjort J (1914) Fluctuations in the great fisheries of Northern Europe viewed in the light of biological research. Rapp P-V Réun Cons Int Explor Mer 20:1–228
Houde ED (2008) Emerging from Hjort's shadow. J Northwest Atl Fish Sci 41:53–70
Iles TD, Sinclair M (1982) Atlantic herring: stock discreteness and abundance. Science 215:627–633
Kendall AW, Ahlstrom EH, Moser HG (1984) Early life history stages of fishes and their characters. In: Moser HG, Richards WJ, Cohen DM, Fahay MP, Kendall AW, Richardson SL (eds) Ontogeny and systematics of fishes. Allen Press, Lawrence, KS, p 11–22
Landaeta MF, Martínez RA, Bustos CA, Castro LR (2013) Distribution of microplankton and fish larvae related to sharp clines in a Patagonian fjord. Rev Biol Mar Oceanogr 48:401–407
Large WG, McWilliams JC, Doney SC (1994) Oceanic vertical mixing: a review and a model with a nonlocal boundary layer parameterization. Rev Geophys 32:363–403
Lasker R (1978) The relations between oceanographic conditions and larval anchovy food in the California Current: identification of factors contributing to recruitment failure. Rapp P-V Réun Cons Int Explor Mer 173:212–230
Leal E, Muñoz C, Moyano G, Bernal C, Aranis A (2017) A first experience of Patagonian sprat *Sprattus fuegensis* spawning in captivity: adult acclimation, egg and larval measurements. Rev Biol Mar Oceanogr 52:641–645
Lebour MV (1921) The larval and post-larval stages of the pilchard, sprat and herring from Plymouth district. J Mar Biol Assoc UK 12:427–457
Lima ARA, Garrido S, Riveiro I, Rodrigues D and others (2022) Seasonal approach to forecast the suitability of spawning habitats of a temperate small pelagic fish

under a high-emission climate change scenario. Front Mar Sci 9:956654

Loeb VJ (1980) Patterns of spatial and species abundance within the larval fish assemblage of the North Pacific central gyre during late summer. Mar Biol 60:189–200

Marchesiello P, McWilliams JC, Shchepetkin A (2001) Open boundary conditions for long-term integration of regional oceanic models. Ocean Model 3:1–20

Matano RP, Combes V, Piola AR, Guerrero R and others (2014) The salinity signature of the cross-shelf exchanges in the Southwestern Atlantic Ocean: numerical simulations. J Geophys Res Oceans 119:7949–7968

Matano RP, Palma ED, Combes V (2019) The Burdwood Bank circulation. J Geophys Res Oceans 124:6904–6926

Milligan S (1986) Recent studies on the spawning of sprat (*Sprattus sprattus*) in the English Channel. Fisheries Research Technical Report No. 83. Ministry of Agriculture, Fisheries and Food, Directorate of Fisheries Research, Lowestoft

Ospina-Alvarez A, Catalán IA, Bernal M, Roos D, Palomera I (2015) From egg production to recruits: connectivity and inter-annual variability in the recruitment patterns of European anchovy in the northwestern Mediterranean. Prog Oceanogr 138:431–447

Ospina-Alvarez A, de Juan S, Alós J, Basterretxea G and others (2020) MPA network design based on graph theory and emergent properties of larval dispersal. Mar Ecol Prog Ser 650:309–326

Palma ED, Matano RP, Piola AR (2008) A numerical study of the Southwestern Atlantic Shelf circulation: stratified ocean response to local and offshore forcing. J Geophys Res Oceans 113:C11010

Palma ED, Matano RP, Combes V (2021) Circulation and cross-shelf exchanges in the Malvinas Islands Shelf region. Prog Oceanogr 198:102666

Parrish RH, Nelson CS, Bakun A (1981) Transport mechanisms and reproductive success of fishes in the California Current. Biol Oceanogr 1:175–203

Peck MA, Huebert KB, Llopiz JK (2012a) Intrinsic and extrinsic factors driving match–mismatch dynamics during the early life history of marine fishes. Adv Ecol Res 47:177–302

Peck MA, Baumann H, Bernreuther M, Clemmesen C and others (2012b) The ecophysiology of *Sprattus sprattus* in the Baltic and North Seas. Prog Oceanogr 103:42–57

Peck MA, Reglero P, Takahashi M, Catalán IA (2013) Life cycle ecophysiology of small pelagic fish and climate-driven changes in populations. Prog Oceanogr 116: 220–245

Perry AL, Low PJ, Ellis JR, Reynolds JD (2005) Climate change and distribution shifts in marine fishes. Science 308:1912–1915

Petereit C, Haslob H, Kraus G, Clemmesen C (2008) The influence of temperature on the development of Baltic Sea sprat (*Sprattus sprattus*) eggs and yolk sac larvae. Mar Biol 154:295–306

Petitgas P, Alheit J, Peck MA, Raab K and others (2012) Anchovy population expansion in the North Sea. Mar Ecol Prog Ser 444:1–13

Piola AR, Gordon AL (1989) Intermediate waters in the southwest South Atlantic. Deep-Sea Res A, Oceanogr Res Pap 36:1–16

R Core Team (2022) R: a language and environment for statistical computing. R Foundation for Statistical Computing, Vienna

Riccialdelli L, Becker YA, Fioramonti NE, Torres M, Bruno DO, Rey AR, Fernández DA (2020) Trophic structure of southern marine ecosystems: a comparative isotopic analysis from the Beagle Channel to the oceanic Burdwood Bank area under a wasp-waist assumption. Mar Ecol Prog Ser 655:1–27

Romagnoni G, Kvile KØ, Dagestad KF, Eikeset AM, Kristiansen T, Stenseth NC, Langangen Ø (2020) Influence of larval transport and temperature on recruitment dynamics of North Sea cod (*Gadus morhua*) across spatial scales of observation. Fish Oceanogr 29:324–339

Sánchez RP, Ciechomski JD (1995) Spawning and nursery grounds of pelagic fish species in the sea-shelf off Argentina and adjacent areas. Sci Mar 59:455–478

Sánchez RP, Remeslo A, Madirolas A, de Ciechomski JD (1995) Distribution and abundance of post-larvae and juveniles of the Patagonian sprat, *Sprattus fuegensis* and related hydrographic conditions. Fish Res 23:47–81

Sánchez RP, Madirolas A, Reta R, Ehrlich MD, Álvarez Colombo G, Macchi G (1997) The reproductive biology of the Patagonian sprat (*Sprattus fuegensis*): several facts and still some speculations. ICES CM 1997/HH:22

Sandvik H, Barrett RT, Erikstad KE, Myksvoll MS and others (2016) Modelled drift patterns of fish larvae link coastal morphology to seabird colony distribution. Nat Commun 7:11599

Schlag Z, North EW, Smith K (2008) Larval TRANSport Lagrangian model (LTRANS) user's guide. University of Maryland Center for Environmental Science, Horn Point Laboratory, Cambridge, MD

Smagorinsky J (1963) General circulation experiments with the primitive equations: I. The basic experiment. Mon Weather Rev 91:99–164

Spinelli ML, Malits A, García Alonso VA, Martín J, Capitanio FL (2020) Spatial gradients of spring zooplankton assemblages at the open ocean sub-Antarctic Namuncurá Marine Protected Area/Burdwood Bank, SW Atlantic Ocean. J Mar Syst 210:103398

Strub PT, James C, Combes V, Matano RP and others (2015) Altimeter-derived seasonal circulation on the southwest Atlantic shelf: 27°–43°S. J Geophys Res Oceans 120: 3391–3418

Suca JJ, Ji R, Baumann H, Pham K and others (2022) Larval transport pathways from three prominent sand lance habitats in the Gulf of Maine. Fish Oceanogr 31: 333–352

Torrado H, Mourre B, Raventos N, Carreras C, Tintoré J, Pascual M, Macpherson E (2021) Impact of individual early life traits in larval dispersal: a multispecies approach using backtracking models. Prog Oceanogr 192:102518

Vasconcellos M, Csirke J (2011) B6. Southwest Atlantic. In: Review of the state of world marine fishery resources. Fisheries and Aquaculture Technical Paper No. 569. FAO, Rome, p 93–105

Visser AW (1997) Using random walk models to simulate the vertical distribution of particles in a turbulent water column. Mar Ecol Prog Ser 158:275–281

Whitehead PJP (1985a) An annotated and illustrated catalogue of herrings, sardines, pilchards, sprats, shads, anchovies and wolf-herrings. Clupeoid fishes of the world (suborder Clupeoidei). FAO Fish Synop 125: 305–579

Whitehead PJP (1985b) King herring: his place amongst the clupeoids. Can J Fish Aquat Sci 42:s3–s20

Appendix.

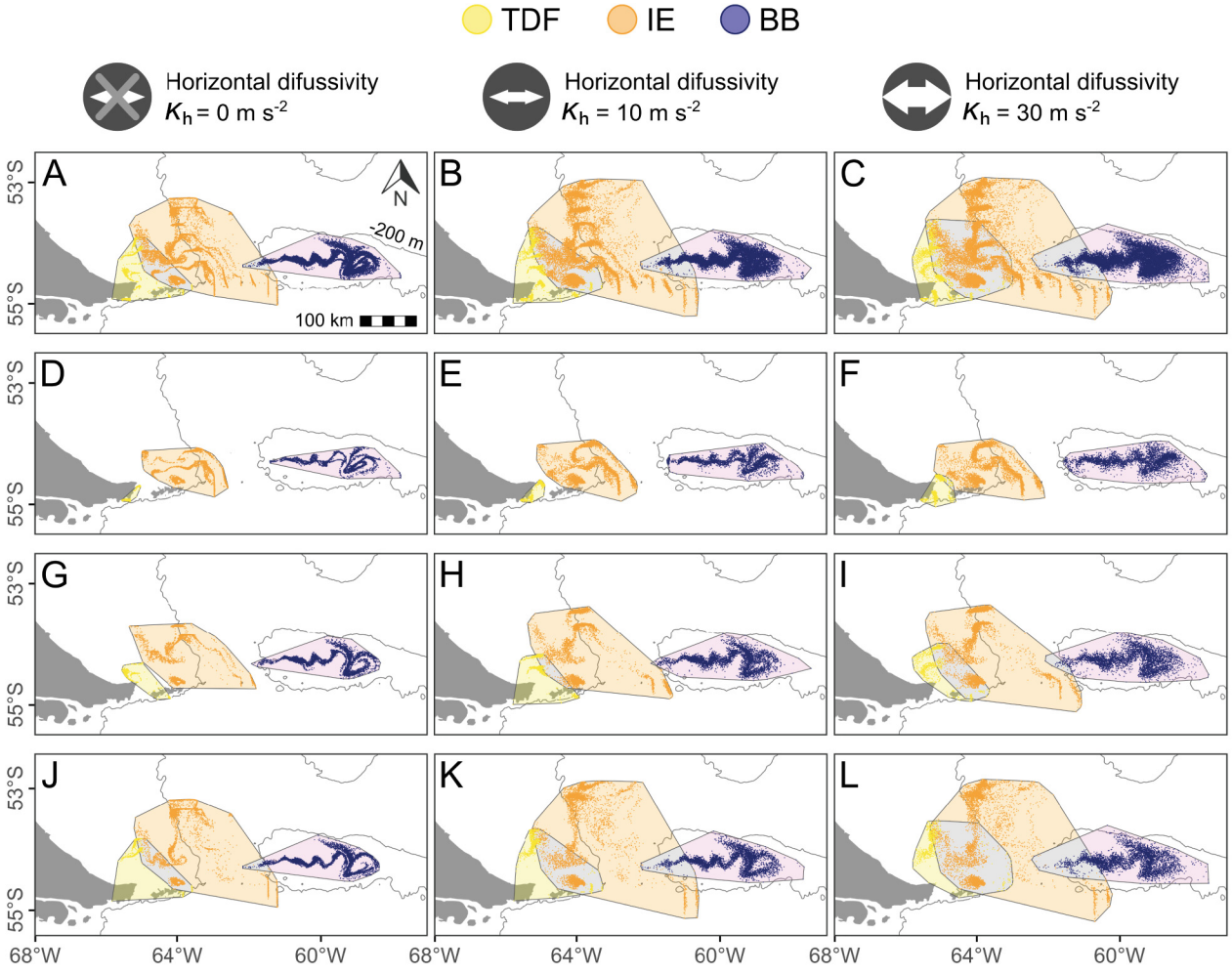

Fig. A1. Visual representation of the general methodology employed to estimate connectivity among neighbouring areas. Polygons covering all particles for each zone were generated (coloured according to the zone), the extension of overlapping areas among polygons were calculated, and connectivity was quantified as the percentage of particles in overlapping areas (polygons with grey background) in comparison to the total number of particles released from the 2 areas considered in each case. Estimations were repeated for simulations performed with (K_h = 10 and 30 m s^{-2}) and without (K_h = 0 m s^{-2}) horizontal diffusivity considering the final position of all particles (overall) and according to the month of release (October, November, and December) in austral spring. TDF: Tierra del Fuego; IE: Isla de los Estados; BB: Burdwood Bank

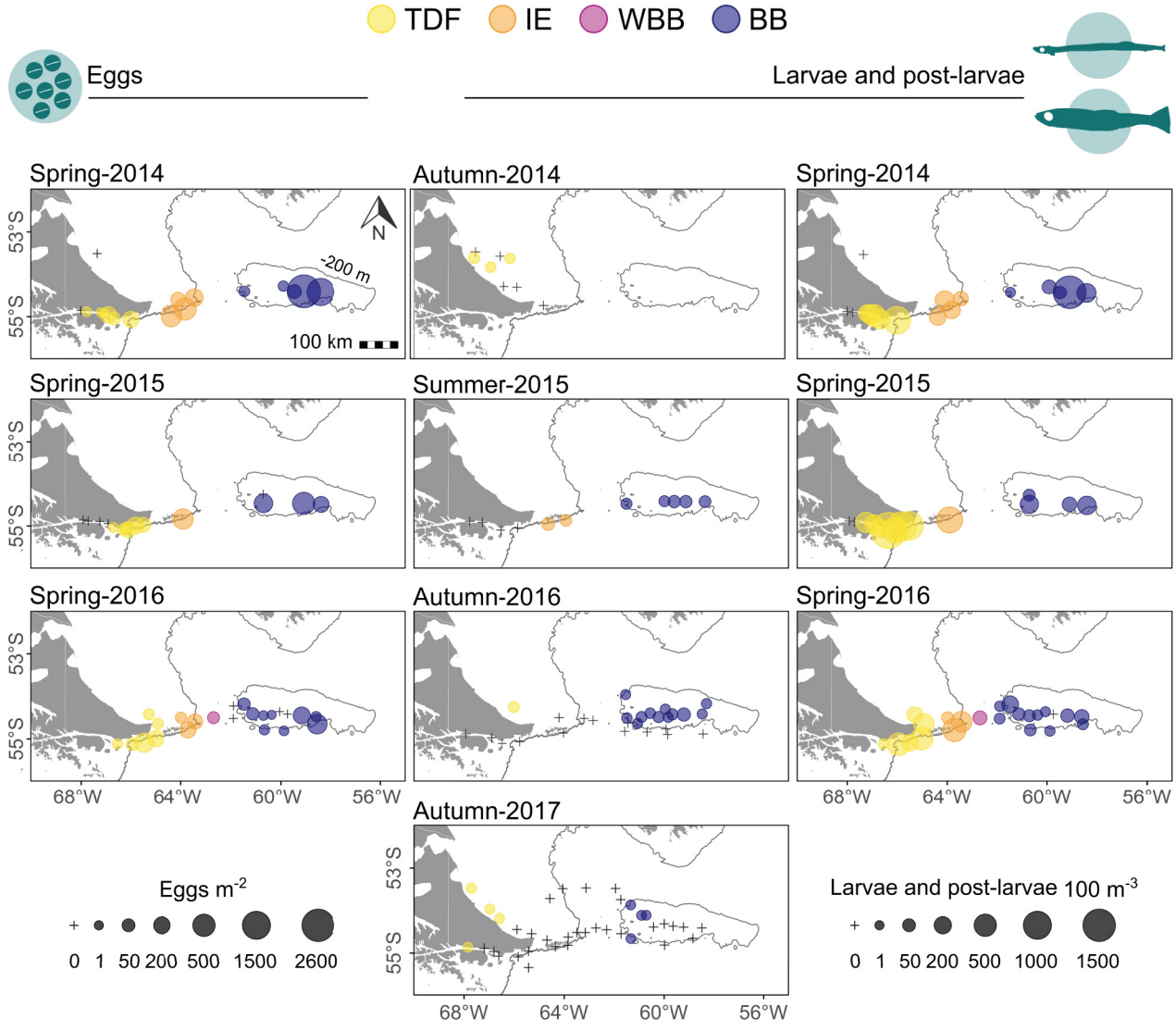

Fig. A2. Distribution and abundance of Fuegian sprat early life stages according to the oceanographic survey analysed. Left-hand panels refer to eggs found during spring surveys, while middle and right-hand panels refer to larvae and postlarvae found during all surveys. TDF: Tierra del Fuego; IE: Isla de los Estados; WBB: West Burdwood Bank; BB: Burdwood Bank

Editorial responsibility: Alejandro Gallego, Aberdeen, UK
Reviewed by: T. Dobbelaere, J. J. Suca and 1 anonymous referee

Submitted: June 14, 2022
Accepted: May 15, 2023
Proofs received from author(s): June 30, 2023